39

High Energy-Loss Spectra and Images

CHAPTER PREVIEW

The high energy-loss spectrum ($\mathcal{E} > 50$ eV) consists primarily of ionization or core-loss edges on a rapidly decreasing plural-scattering background. Elemental-composition data and elemental maps can be extracted from these ionization edges. In this chapter, we'll examine how to get this information, quantify it, and image it. A good use for such data is light-element analysis wherein EELS complements XEDS. First, we'll remind you of the experimental variables over which you have control, because these are rather critical. Then we'll discuss how to obtain a spectrum and what it should look like if you're going to quantify it. Next, we'll discuss the various quantification routines which, in principle, are just as straightforward as those for XEDS but in practice require rather more sophisticated software, and we often need to use deconvolution routines. Elemental imaging is a powerful aspect of high-energy-loss EELS, particularly, because both the spatial resolution and minimum detection limits are somewhat better than XEDS and atomic-column spectroscopy and single-atom detection are more easily achievable in EELS.

39.1 THE HIGH-LOSS SPECTRUM

The high-loss portion of the spectrum above ~50 eV contains information from inelastic interactions with the inner or core shells. These interactions provide direct elemental identification in a manner similar to XEDS and other information, such as bonding and atomic position. We'll emphasize quantitative elemental analysis and mapping in this chapter and discuss the other features of the high-loss spectrum in the next chapter.

39.1.A Inner-Shell Ionization

When a beam electron transfers sufficient energy to a core-shell electron (i.e., one in the inner, more tightly bound K, L, M, etc., shells) to move it outside the attractive field of the nucleus, the atom is said to be ionized (go back and look at Figure 4.2). As you know from the earlier chapters on X-ray analysis, the decay of the excited atom back to its ground state may produce a characteristic X-ray or an Auger electron. So high-loss EELS and XEDS detect different aspects of the same phenomenon. Ionization is the primary event and X-ray emission is one of two secondary processes. We are interested in ionization losses precisely because the process is characteristic of the atom involved and so the signal is a direct source of chemical information, just like the characteristic X-ray. We call the ionization-loss signal in the EELS spectrum an 'edge,' rather than a peak, for reasons we'll describe shortly and we use the edges as the basis for elemental mapping.

EELS COMPLEMENTS XEDS

Detection of the high-energy electron that ionized the atom is independent of whether the atom emits an X-ray or an Auger electron. So EELS is **not** affected by the fluorescence-yield limitation that restricts light-element X-ray analysis. These differences explain, in part, the complementary nature of XEDS and ionization-loss EELS but also the much higher efficiency of EELS.

Ionization is a relatively high-energy process. For example, the lightest solid element, Li, requires an input of ~55 eV to eject a K-shell electron, and so the loss electrons are usually found in the high-loss region of the spectrum, above $\mathcal{E} = 50$ eV. K-shell electrons require much more energy for ejection as Z increases because they are more strongly bound to the nucleus. The binding energy for electrons in the uranium K shell is about 99 keV. So we tend to use L and M edges when dealing with high-Z atoms (just like in XEDS) because the intensity of the K edges decreases substantially above ~2 keV. It's worth a short mention here about the nomenclature used

for EELS edges. As for X-rays, where we have K, L, M, etc., peaks in the spectrum, we get ionization edges from K, L, M, etc., shell electrons. However, the much better energy resolution of the magnetic-prism spectrometer means that it is much easier to detect small differences in spectra that arise from the presence of different energy states in the shell. For example

- The K shell electron is in the 1 s state and gives rise to a single K edge.
- In the L shell, the electrons are in either 2s or 2p orbitals, and if a 2s electron is ejected, we get an L_1 edge and a 2p electron causes either an L_2 or L_3 edge.

Depending on the ionization energy, the L_2 and L_3 edges may not be resolvable (they aren't in Al but they are in Ti), and so we call this edge the $L_{2,3}$. The full range of possible edges is shown schematically in Figure 39.1, and you can see that other dual edges exist, such as the $M_{4,5}$.

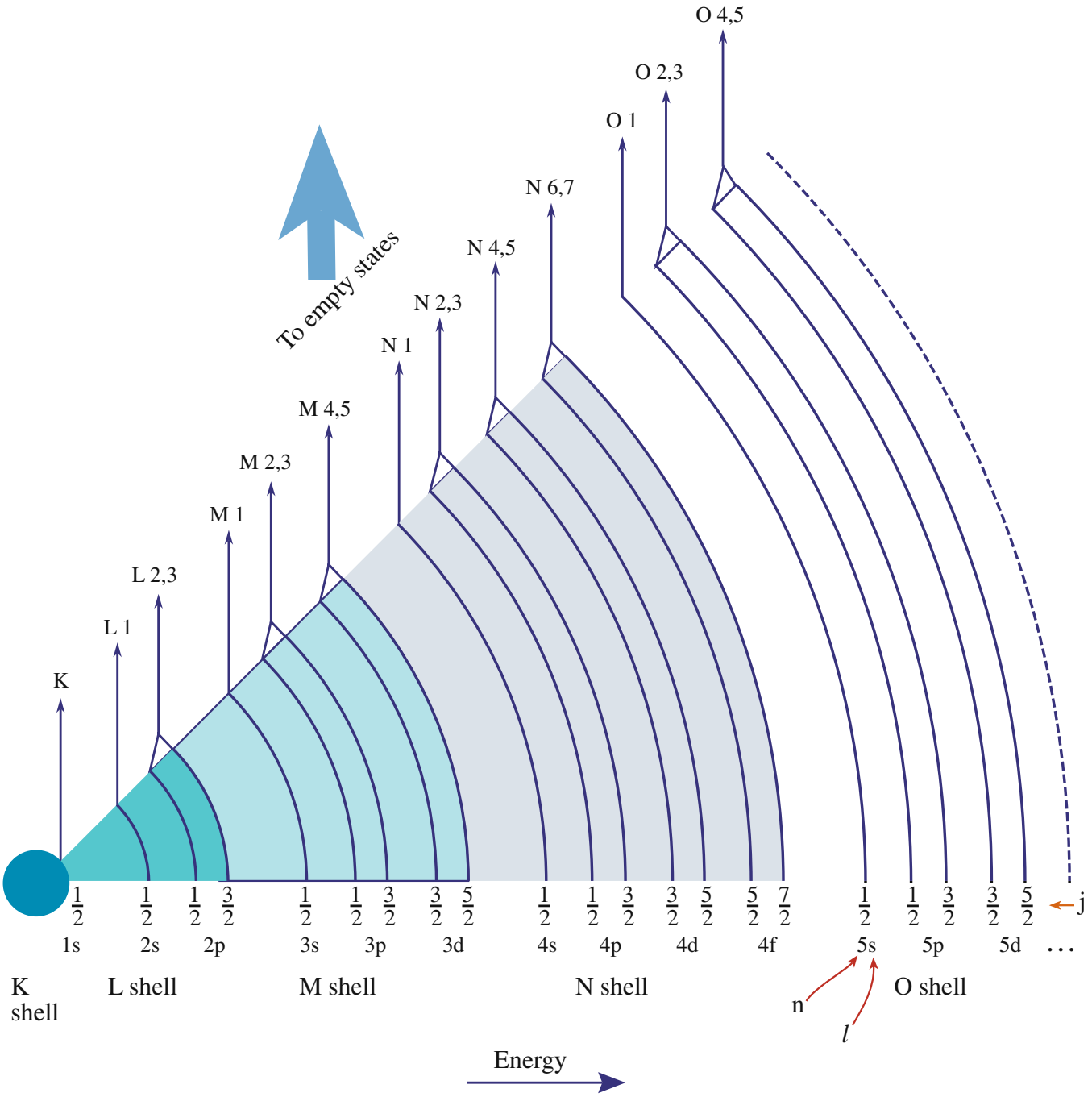

FIGURE 39.1. The full range of possible edges in the energy-loss spectrum due to core-shell ionization and the associated nomenclature.

Compared with plasmon excitation, which requires much less energy, the ionization cross sections are relatively small and the mean free paths relatively large. As a result, the ionization-edge intensity in the spectrum is much smaller than the plasmon peak, and becomes even smaller as the energy loss increases (look back to Figure 37.1). This is another reason for staying with the lower energy-loss (L and M) core edges. While the possibility of plural ionization events being triggered by the same electron is small in a typical thin foil, we'll see that the combination of an ionization loss and a plasmon loss is by no means uncommon. This phenomenon distorts the EEL spectrum and any filtered images.

If you go back and look at Figure 4.2, you can see that a specific minimum-energy transfer from the beam electron to the inner-shell electron is required to overcome the binding energy of the electron to the nucleus and ionize the atom. This minimum energy constitutes the ionization threshold, or the critical ionization energy, E_c.

We define E_C as E_K for a particular K-shell electron, E_L for an L shell, etc. Of course, it is also possible to ionize an atom by the transfer of $\mathcal{E} > E_C$. However, the probability of ionization occurring becomes less with increasing energy above E_C because the ionization cross section decreases with increasing energy transfer. As a result, the ionization-loss electrons have an energy distribution that ideally shows a sharp rise to a maximum at E_C, followed by a slowly decreasing intensity above E_C back toward the background. This triangular shape is called an edge because you'll notice that, as shown in Figure 39.2A, it has a similar intensity profile to the absorption edges in X-ray spectroscopy. Often the term 'hydrogenic' is used for such a sharp edge-onset because this is what would arise from the ionization of the ideal single isolated hydrogen atom.

TRIANGULAR SHAPE

This idealized triangular or sawtooth shape is only found in spectra from isolated hydrogen atoms and is therefore called a hydrogenic ionization edge. Real ionization edges have shapes that approximate, more or less, to the hydrogenic edge.

In reality, because we aren't dealing with isolated atoms, but atoms integrated into a crystal lattice or an amorphous structure, the spectra are more complex. Ionization edges are superimposed on a rapidly decreasing background intensity from electrons that have undergone random, plural inelastic scattering events (Figure 39.2B). The edge may also show fine structure oscillations within ~50 eV of E_C (Figure 39.2C) which are due to bonding effects (termed energy-loss near-edge structure, ELNES). More than 50 eV after the edge, small intensity oscillations may be detectable (Figure 39.2D) due to diffraction effects from the atoms surrounding the ionized atom, and these are called extended energy-loss fine structure (EXELFS), which is analogous to extended X-ray absorption fine structure (EXAFS) in X-ray spectra, particularly, those generated from intense synchrotron sources.

ELNES AND EXELFS

Fine structure around the ionization edge onset is known as ELNES. Small intensity oscillations >~50 eV after the edge due to diffraction effects are called EXELFS.

Finally, as we noted earlier, the ionization-loss electrons may also undergo low-loss interactions. For example, they may create plasmons, in which case the edge contains extra plural-scattering intensity ~15–25 eV above E_C, as shown schematically in Figure 39.2E. So experimental ionization edges are far more complicated than the Gaussian peaks in an XEDS spectrum, but they also contain far more information about the specimen than a characteristic peak. From an XEDS spectrum, you only get *elemental* identification rather than *chemical* information, such as bonding which is contained both in the ELNES and the low-loss structure (although as we showed in Figure 32.9C, if the X-ray spectrometer has sufficiently high-energy resolution, it can detect such differences but the price to pay in the AEM is an unacceptably low count rate). Figure 39.3 shows a spectrum from BN on a C film. The various ionization edges show some of the features drawn schematically in Figure 39.2, in particular, strong ELNES on the B-K edge; we'll discuss these fine-structure effects more in Section 40.1 and how to form fine-structure images from them in Section 40.5.C.

39.1.B Ionization-Edge Characteristics

The angular distribution of ionization-loss electrons varies as $(\theta^2 + \theta_E^2)^{-1}$ and will be a maximum when $\theta = 0$, in the forward-scattered direction. The distribution decreases to a half width at the characteristic scattering angle θ_E given by equation 38.1. This behavior is essentially the same as for plasmon scattering but because we have relatively large values of E_C compared to E_P, we get larger characteristic scattering angles for ionization-loss electrons (e.g., for the typical, maximum core-loss energy that we would use for analysis $\mathcal{E} = 2000$ eV so $\theta_E \sim 10$ mrad when $E_0 = 100$ keV).

The angular distribution varies depending on $\mathcal{E}$, and because of the extended energy range of ionization-loss

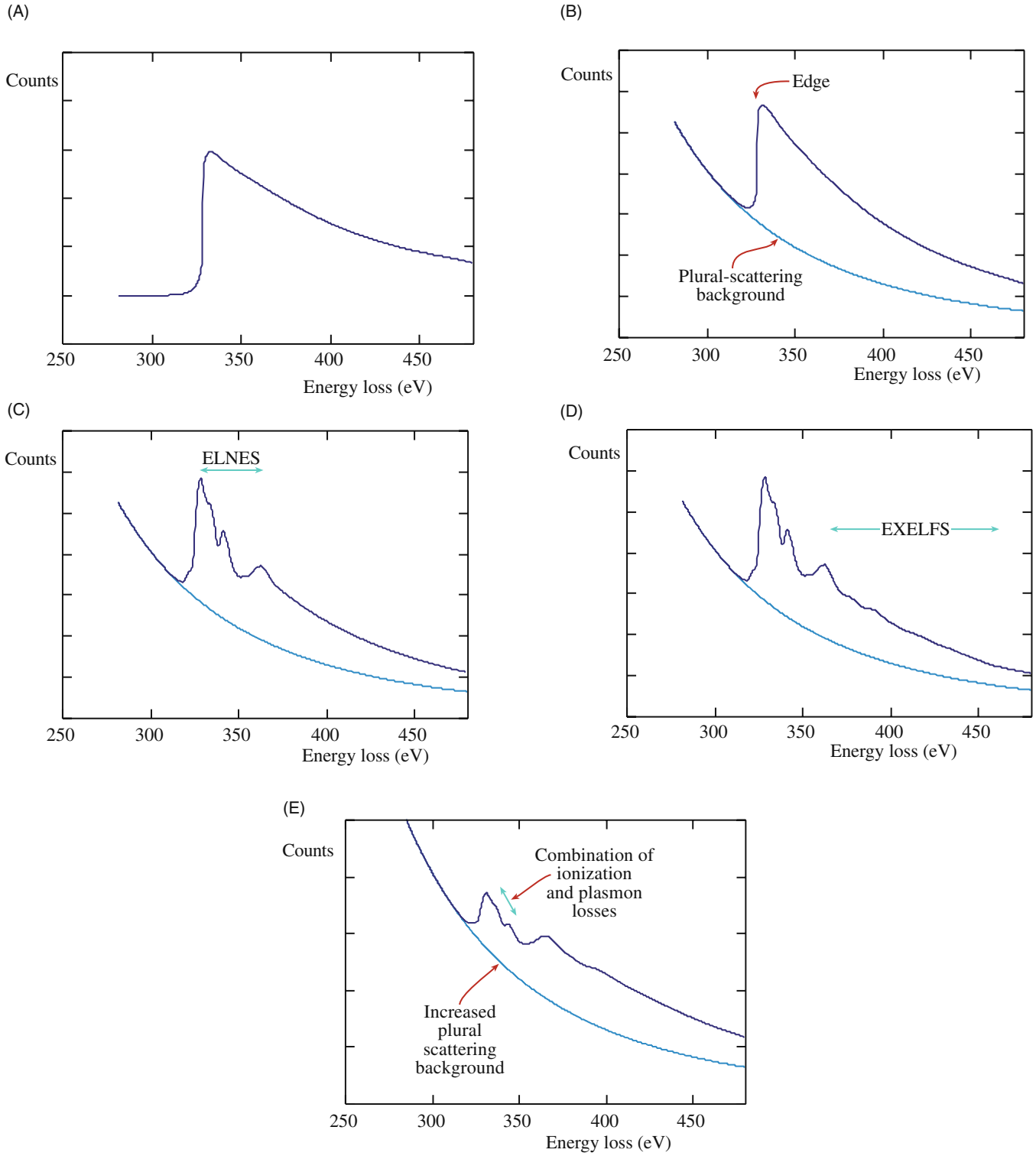

FIGURE 39.2. The characteristic features of an inner-shell ionization edge. (A) The idealized sawtooth (hydrogenic) edge. (B) The hydrogenic edge superimposed on the background arising from plural inelastic scattering. (C) The presence of ELNES. (D) The EXELFS. (E) In a thick specimen, plural scattering, such as the combination of ionization and plasmon losses, adds another peak to the post-edge structure and raises the background level.

electrons above E_C, this can be quite complicated. For $\mathcal{E} \sim E_C$ the scattering intensity drops rapidly to zero over about 10 mrads (at θ_e), but as $\mathcal{E}$ increases above E_C the angular-intensity distribution drops around $\theta = 0°$, but increases at larger scattering angles, giving rise to the so-called Bethe ridge. However, this effect is not really important for the kind of analytical studies that we are emphasizing in this chapter.

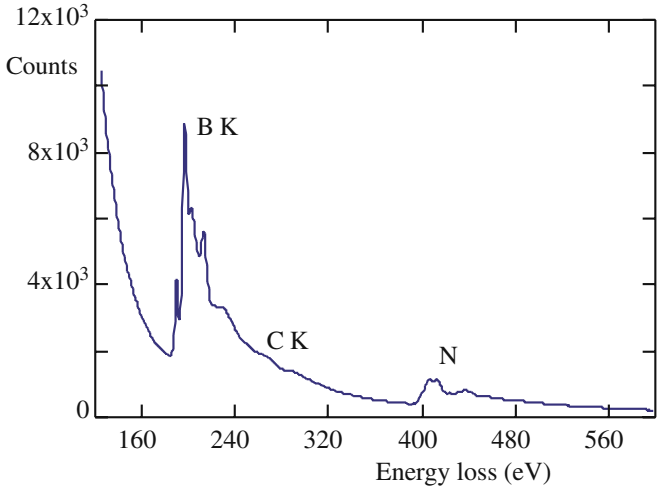

FIGURE 39.3. High energy-loss spectrum from a thin flake of BN sitting on the edge of a hole in an amorphous-carbon support film. The B K and N K edges are clearly visible superimposed on a rapidly decreasing background. A very small C K edge is also detectable at ~280 eV.

So, the distribution of characteristic scattering angles for the core-loss electrons that we use for analysis span the range from ~0.2 to 10 mrads and the scattering cut-off angles range from ~25 to 200 mrads (equation 38.4). In other words, like the plasmon-loss electrons, the ionization-loss electrons are very strongly forward-scattered. Consequently, efficient collection of most inelastically scattered electrons is straightforward, since a spectrometer entrance aperture angle (β) of 10 mrads will collect the great majority of such electrons. As a result, collection efficiencies in the range 50–100% are not unreasonable, which contrasts with XEDS where the isotropic generation of characteristic X-rays results in very inefficient collection. Figure 39.4 compares the collection of X-rays and energy-loss electrons and Figure 39.5 shows the variation in collection efficiency for ionization-loss electrons as a function of both β and energy.

While the K edges in Figure 39.3 show sharp onsets, like an ideal hydrogenic edge, not all edges are similar in shape. Some edges have much broader onsets, spread over several eV or even tens of eV. The edge shape in general depends on the electronic structure of the atom but, unfortunately, we can't give a simple relationship between edge types and specific shapes. The situation is further complicated because the edge shapes change depending on whether or not certain energy states are filled or unfilled. For example, if you go back and look at Figure 37.1, the Ni L edge shows two sharp peaks, which are the L_3 and L_2 edges. (We'll discuss these details much more in Section 40.1.) These sharp lines arise because the ejected L shell electrons don't entirely escape from the atom and have a very high probability of ending up in unfilled d-band states. In contrast, in Cu where the d band is full, the $L_{2,3}$ edge does not show these intense lines. Similar sharp lines appear in the $M_{4,5}$ edges in the rare earths. As if this were not enough, the

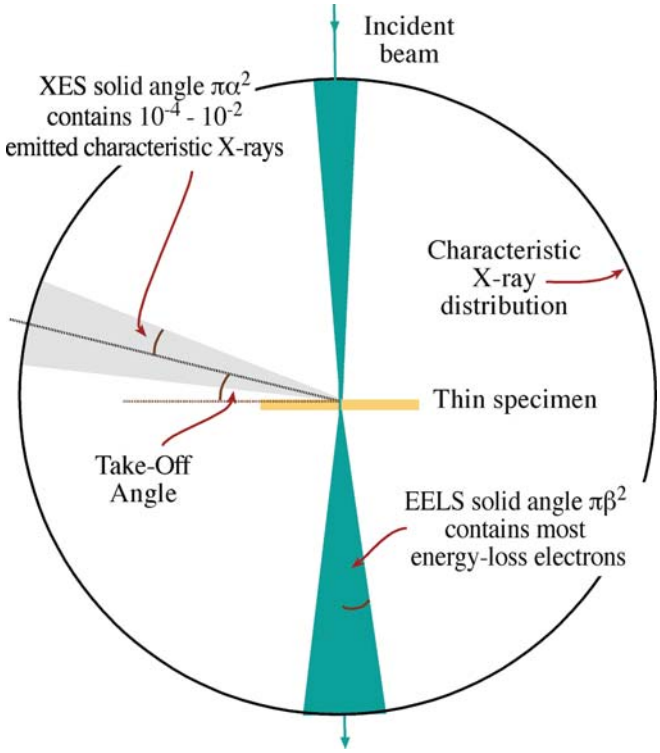

FIGURE 39.4. Comparison of the relative efficiencies of collection of EELS and XES. The forward-scattered energy-loss electrons are very efficiently collected with even a small EELS collection angle. In contrast, only a small fraction of the uniformly emitted (4π sr) characteristic X-rays is detected by the XEDS.

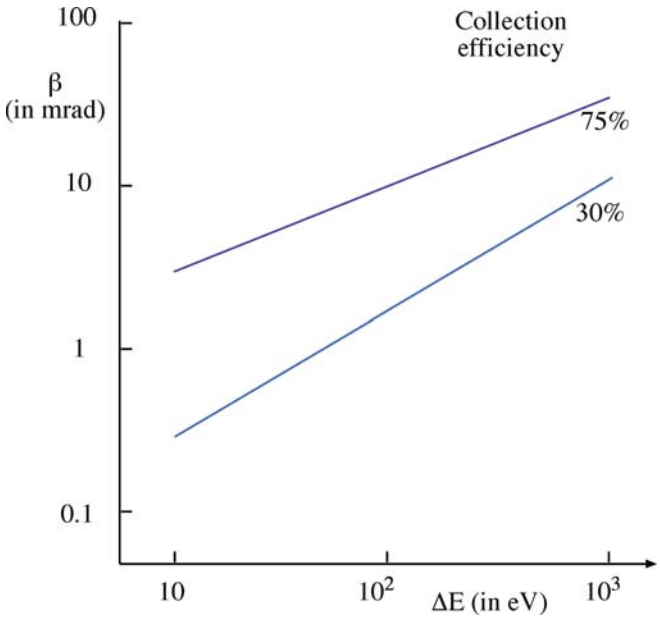

FIGURE 39.5. Variation in the collection efficiency of ionization-loss electrons as a function of energy loss and spectrometer collection angle. A 10 mrad collection angle will gather over 75% of all the incident-beam electrons that ionized C atoms and lost ~285 eV.

details of the fine structure and edge shapes are also affected by bonding. For example, the Si edge in a spectrum from SiO_2 is different from the Si edge from pure Si. To sort all this out it's best if you consult the 2004 EELS Atlas (by Ahn and related references in the previous chapter) which contains representative edges from all the elements and many oxides.

Now that we've covered both the low and high energy-loss processes, we can summarize the characteristics of the energy-loss spectrum by examining a complete spectrum from NiO containing both low and high-loss electrons, as shown in Figure 39.6. In this figure, we also compare the spectrum to the energy-level diagram for NiO. You can see that

- The ZLP is above the potential wells since these electrons don't interact with the atom.
- The plasmon peak comes from interactions with the valence/conduction band electrons just below the Fermi level (E_F).

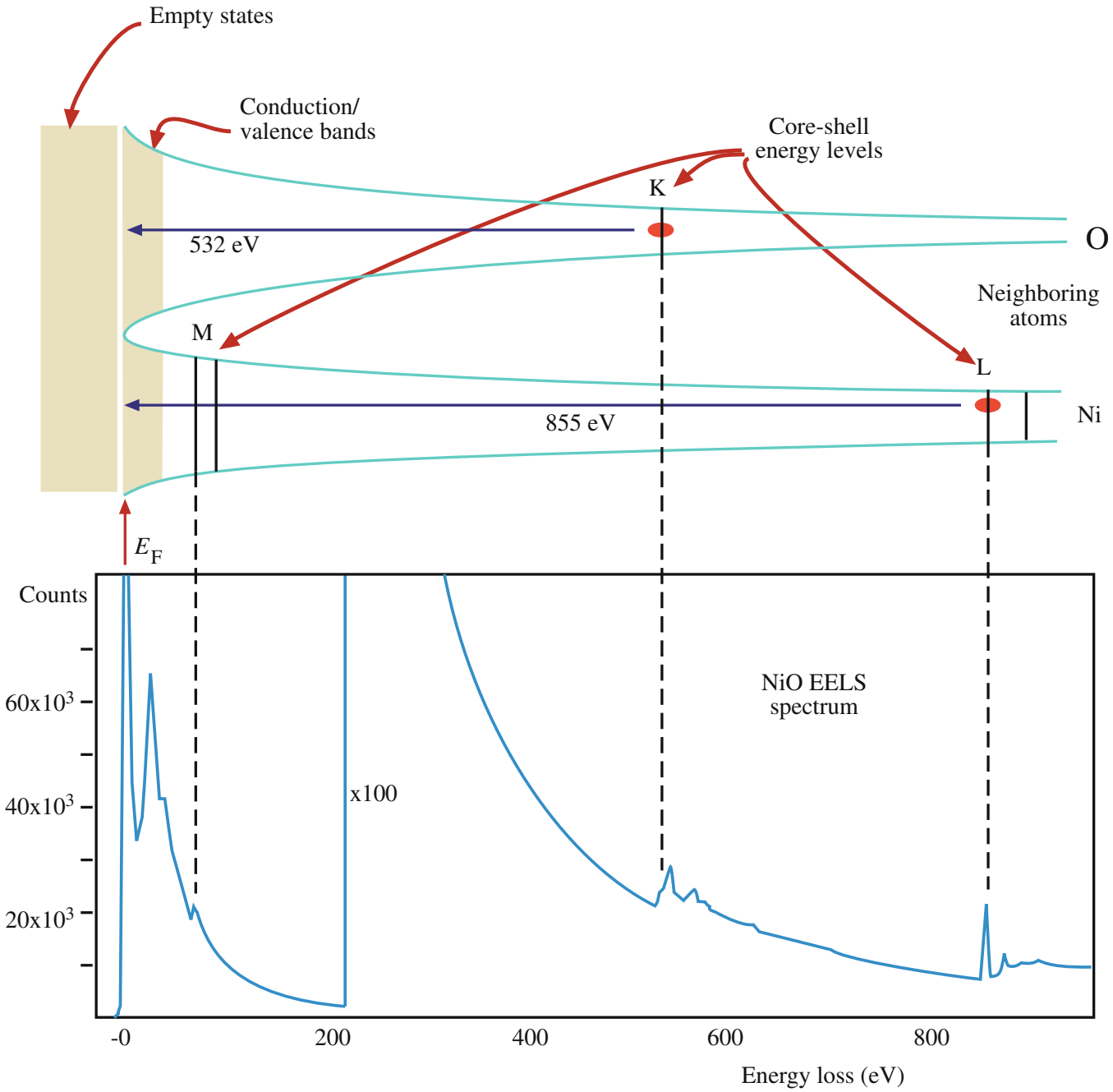

FIGURE 39.6. The correspondence between the energy levels of electrons surrounding adjacent Ni and O atoms and the energy-loss spectrum. The deeper the electrons sit in the potential well the more the energy needed to eject them. The ZLP is above the Fermi energy E_F, the plasmon peak is shown at the energy level of the conduction/valence bands where plasmon oscillations occur in the loosely bound electrons. The critical ionization energy required to eject electrons in specific shells is shown (Ni L: 855 eV and O K: 532 eV).

- The relative energy levels of the ionized shell (K, L, or M) control the position of the ionization edge in the spectrum. The closer to the nucleus, the deeper the potential well and the more the energy required to eject the electron.
- There will be a different density of states in the valence (3d) band of the Ni atom compared to the s band of the O atoms at the top of the potential wells.
- The core electrons could also be given enough energy to travel into the empty states, well above E_F and, in this case, we see ELNES after the ionization edge. We'll discuss more details of such fine structure in the spectrum in Chapter 40.

Despite the very high collection efficiency of the spectrometer, the ionization edges still show relatively low intensity, particularly as $\mathcal{E}$ increases. The edges have an extended energy range well above E_C and ride on a rapidly varying, relatively high background. All these factors, as we shall see, combine to make quantitative analysis using EELS a little more challenging than XEDS. However, for the lighter elements the X-ray fluorescence yield drops to such low values, and absorption becomes so strong, even in thin specimens, that EELS is the preferred technique. Experimentally, the choice between the two is not always simple, but below oxygen in the periodic table, EELS shows better performance than XEDS and for elements below boron, there is no sensible alternative to EELS for nanometer-scale analysis.

39.2 ACQUIRING A HIGH-LOSS SPECTRUM

From what we've described about the various EEL spectrometers and filters and the complexity of the spectra, it should be clear that there are many variables to control when acquiring a spectrum (see Brydson's monograph for a detailed description). Computer control via the Gatan software now makes this process very straightforward. We'll start by summarizing the major parameters relevant to acquiring high-loss spectra and images and indicate reasonable values for each parameter.

- *Beam Energy* E_0: It's best to use the highest E_0, unless doing so causes displacement damage or significant surface sputtering. A higher E_0 reduces the scattering cross section and so you get reduced edge intensity. Conversely, as E_0 increases, the plural-scattering background intensity falls faster than the edge intensity and so the signal to background increases. The increase in signal to background varies with the particular edge but it is never a strong variation; so while we recommend using the highest kV, it's not a good reason (on its own) to justify purchasing a 300-keV TEM.
- *Convergence angle* α: You know how to control α with the C2 aperture and/or the C2 lens, but α is only important in quantification if it is larger than β. So if you operate in TEM image or diffraction mode with a broad, parallel beam, rather than STEM mode, you can ignore α; otherwise, use the correction factor we give later in Section 39.7.
- *Beam size and current*: You control these factors by your choice of electron source, C1 lens, and C2 aperture. As usual, the beam size is important in determining spatial resolution in STEM mode, and the beam current controls the signal intensity.
- *Specimen thickness*: The specimen must be thin because this minimizes plural-scattering contributions to the spectrum and quantification is more straightforward.

SPECIMEN THICKNESS
Making your specimen as thin as possible is the most important part of EELS.

If your specimen is too thick then you'll have to use deconvolution procedures to remove the effects of plural scattering. So we'll tell you more about how to determine your specimen thickness from the spectrum and how to decide if you need to deconvolute the spectrum.

- *Collection angle* β: You know from Section 37.4 how to measure β in all operating modes. If you need lots of intensity and are happy with poor spatial resolution, use TEM image mode with no objective aperture ($\beta > \sim 100$ mrads). A small spectrometer entrance aperture ensures good energy resolution at the same time. If you want a small β to prevent contributions to the spectrum from high-angle scattering, use diffraction mode (TEM or STEM) and keep the small entrance aperture for good energy resolution. In the STEM case you also get good spatial resolution.

ENTRANCE APERTURE
Remember that a 5 mm diameter entrance aperture gives $\beta \sim 5$ mrad at a camera length of ~ 800 mm.

Generally, for analysis $\beta \sim 1$–10 mrads is fine, so long as it's less than the Bragg angle for your specimen orientation; but for EELS imaging, which we discuss in Section 39.9, 100 mrads may be necessary to get the necessary signal intensity.

- *Energy resolution*: ΔE is limited by your electron source unless you have a monochromator. Elemental analysis and imaging (the topic of this chapter) do not require the best ΔE, so ~5 eV would suffice. You really need the best ΔE for low-loss and fine-structure studies, which are probably the most useful and widespread aspect of EELS (see the surrounding chapters). Use an FEG source and a PEELS/imaging filter if you want to do this, especially if you're lucky enough to have access to a monochromator.
- *Energy-loss range and spectrum dispersion*: The full spectrum extends out to the beam energy E_0, but the useful portion only extends to ~2 keV. Above this $\mathcal{E}$, the intensity is very low, and XEDS is both easier and more accurate. Since you rarely need to collect a spectrum above ~2 keV a minimum of 2048 channels in the computer display, giving 1 eV/channel is a good starting dispersion. You can easily select a higher display resolution if you want to look at a more limited region of the spectrum or if you want to see detail with ΔE <1 eV. Typically, you're only examining a limited portion of the spectrum anyhow and you set this by putting the necessary voltage on the drift tube or changing the high voltage.
- *Dwell time*: If you have a PEELS with a PDA, set the integration time so that at the maximum intensity you don't saturate the diodes: i.e., stay below 16,000 counts per acquisition in the most intense channel and sum as many spectra as you need to give sufficient counts for analysis.
- *Number of acquisitions*: Again, if you have PEELS/PDA, multiple acquisitions may be necessary to get sufficient counts in the edge, but remember that multiple acquisitions may give rise to minor artifacts, as we discussed in Section 37.5.

Before you analyze a particular spectrum, you should check four things

- Focus and align the ZLP and check the spectrometer resolution.
- Look at the low-loss (plasmon) portion of the spectrum; this gives you an idea of your specimen thickness.
- Look for the expected ionization edges. If you can't see any edges, your specimen is probably too thick or you need to raise the display gain.
- It's probably worth deconvoluting out the PSF prior to any quantification.

The first of these tasks is not critical, as we noted earlier. Regarding the second task, we noted back in Chapter 38 that, to a first approximation, if the plasmon-peak intensity is less than about one tenth the ZLP, then the specimen is thin enough for analysis. Otherwise, you'll probably have to deconvolute plural-scattering effects from your experimental spectrum. For the third task, you should ideally see discrete edges on a smoothly varying background, but you need to see at least a change in slope in the background intensity at the expected E_C. If the background intensity is too noisy it will make quantification more difficult, so acquire sufficient counts to generate a smoothly varying background.

THE JUMP RATIO

An important parameter in determining the quality of your spectrum is the signal-to-background ratio which in EELS we call the jump ratio.

The jump ratio is the ratio of the maximum edge intensity (I_{max}) to the minimum intensity (I_{min}) in the channel preceding the edge onset, as shown in Figure 39.7 (which is a well-defined edge from a suitably thin film of amorphous carbon). If the jump ratio is above ~5, for the carbon K edge at 284 eV from a 50 nm carbon film at 100 kV, then your system is operating satisfactorily. You should keep a standard thin, amorphous-carbon film available as a standard reference specimen and occasionally check that the jump ratio remains the same. We'll see that jump-ratio imaging is one method of acquiring filtered images from ionization edges. The jump ratio increases as E_0 increases. If you can't get such a jump ratio from a standard, thin, carbon film, then probably you need to realign the spectrometer. The actual ionization-loss edges from your real specimen, that you may wish to quantify or use to form images, will probably be nothing like this ideal edge, but the EELS software programs are more than capable of

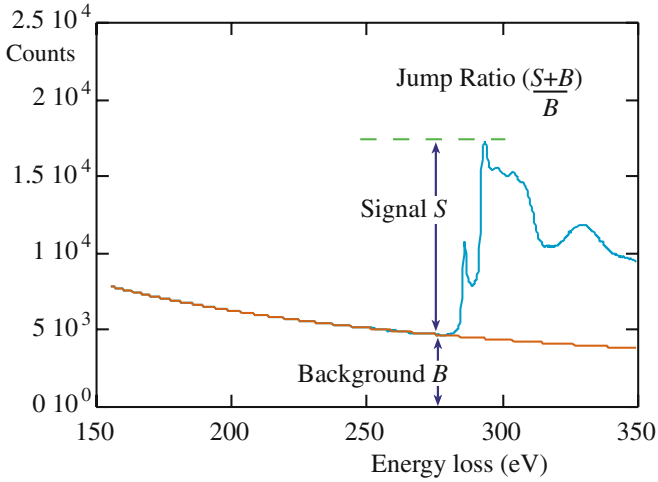

FIGURE 39.7. Definition of the jump ratio of an ionization edge which should be about 5–10 for the carbon K edge if the EELS is well aligned and the specimen really thin. This spectrum shows an adequate jump ratio.

handling much smaller edges riding on much higher backgrounds.

39.3 QUALITATIVE ANALYSIS

As with XEDS, you should always carry out a qualitative analysis first to ensure that you have identified all the features in your spectrum. Then you can decide which edges to use for subsequent quantitative analysis and imaging.

Qualitative analysis using ionization edges is very straightforward. Unlike XEDS, there are actually very few artifacts that can be mistaken for an edge. The most prominent artifact that may lead to misidentification is the ghost peak from diode saturation (see Section 37.5) which is easily removed. So long as you calibrate the spectrum to within a few eV you can unambiguously identify the edge energy.

IONIZATION EDGE

We identify the ionization edge as the energy loss at which there is a discrete increase in the slope of the spectrum; this value is the edge onset, i.e., E_C, the critical ionization energy.

You have to be careful here: sometimes you'll see the edge energy defined somewhat arbitrarily halfway up the edge, e.g., at the π* peak on the front of a C-K edge. There is no strict convention, and very often L and M edges do not have sharp onsets anyhow. Examination of a portion of a spectrum, such as that shown back in Figure 39.3, is usually sufficient to let you draw a definite conclusion about the identity of the specimen, which in this case is BN on a C support film. In addition, it is wise to compare your spectrum with reference spectra from the EELS Atlas that we've mentioned several times before or through an on-line database, such as URL #1.

Remember that there are families of edges (K, $L_{2,3}$, $M_{4,5}$, etc.) just as there are families of peaks in X-ray spectra but, as with X-ray spectra, you might not be able to resolve all the edges in a single family. Given that above ~2 keV the edges are usually too small to be detected, it is in fact very rare that you would expect to see more than one family of lines from a given element (the Si L edge at ~100 eV and the Si K edge at 1.7 keV should both be visible in the same spectrum). As a rule of thumb, quantification is equally easy with K and L edges, but the accuracy of K-edge quantification is slightly better. Up to $Z = 13$ (Al) we usually use K edges because any L edges occur at very low energy and are masked by the plasmon peak. Above $Z = 13$ you can use either K or L edges. Sometimes there is the question of which edge is most visible. The K edge onset is generally a bit sharper than the L edge which consists of both the L_2 and L_3 edges and so may be somewhat broader, but this is not always the case.

L edges for $Z = 19$–28 (e.g., the Ca-L edge in Figure 37.12 and the Cr-L edge in Figure 39.13) and $Z = 37$–45 are characterized by intense near-edge structure called white lines. M edges for $Z = 55$–69 have similar intense lines.

These white lines are so named because they appeared as lines of varying intensity in photographically recorded, energy-loss spectra; they also appear that way if you look at the spectra from in-column filters (see Figure 37.14A). More details will be given in Section 40.1. If you have to use the M, N, or O edges without any white lines, you should know that they are very broad, with an ill-defined threshold, and quantification is best achieved with standards, as we'll see shortly.

The energy-loss spectrum clearly does not lend itself to a quick 'semi-quantitative' analysis; so we can't follow our XEDS approach. For example, the spectrum in Figure 39.3 comes from equal numbers of B and N atoms, but the intensities in the B and N edges are markedly different. This difference arises because of the variation in ionization cross section with $\mathcal{E}$, the strongly varying nature of the plural-scattering background, and the edge shape, which causes the C and N K edges to ride on the tails of the preceding edge(s).

The Ti-nitride and Ti-carbide example: Sometimes qualitative analysis is often all that you need to do. Figure 39.8 shows images and spectra from two small precipitates in an alloy steel. The spectra show a Ti L_{23} edge in both cases and C and N K edges in Figure 39.8A and B, respectively. It does not take much effort to deduce that the first particle is TiC because it is the only known carbide of Ti, but the nitride could be either TiN or Ti_3N. To determine which of the two it is, you have to carry out full quantification, which we'll discuss shortly. You should note that such clear discrimination between TiC and TiN in Figure 39.8B would be difficult using windowless XEDS because the energy resolution is close to the separation of the Ti L ($\mathcal{E}$ = 452 eV) and the N K ($\mathcal{E}$ = 392 eV) X-ray peaks. In addition, the DPs from both phases are almost identical, so this problem is a perfect one for EELS.

39.4 QUANTITATIVE ANALYSIS

To quantify the spectrum or to form a quantitative image, you have to integrate the intensity (I) in the ionization edge(s) by removing the plural-scattering background. Then you have to determine the number of atoms (N) responsible for I. N is related to I by a sensitivity factor termed the partial ionization cross section (σ). We'll see that σ plays a similar role to the k_{AB} factor in X-ray analysis. If you go back and look at Figure 39.2,

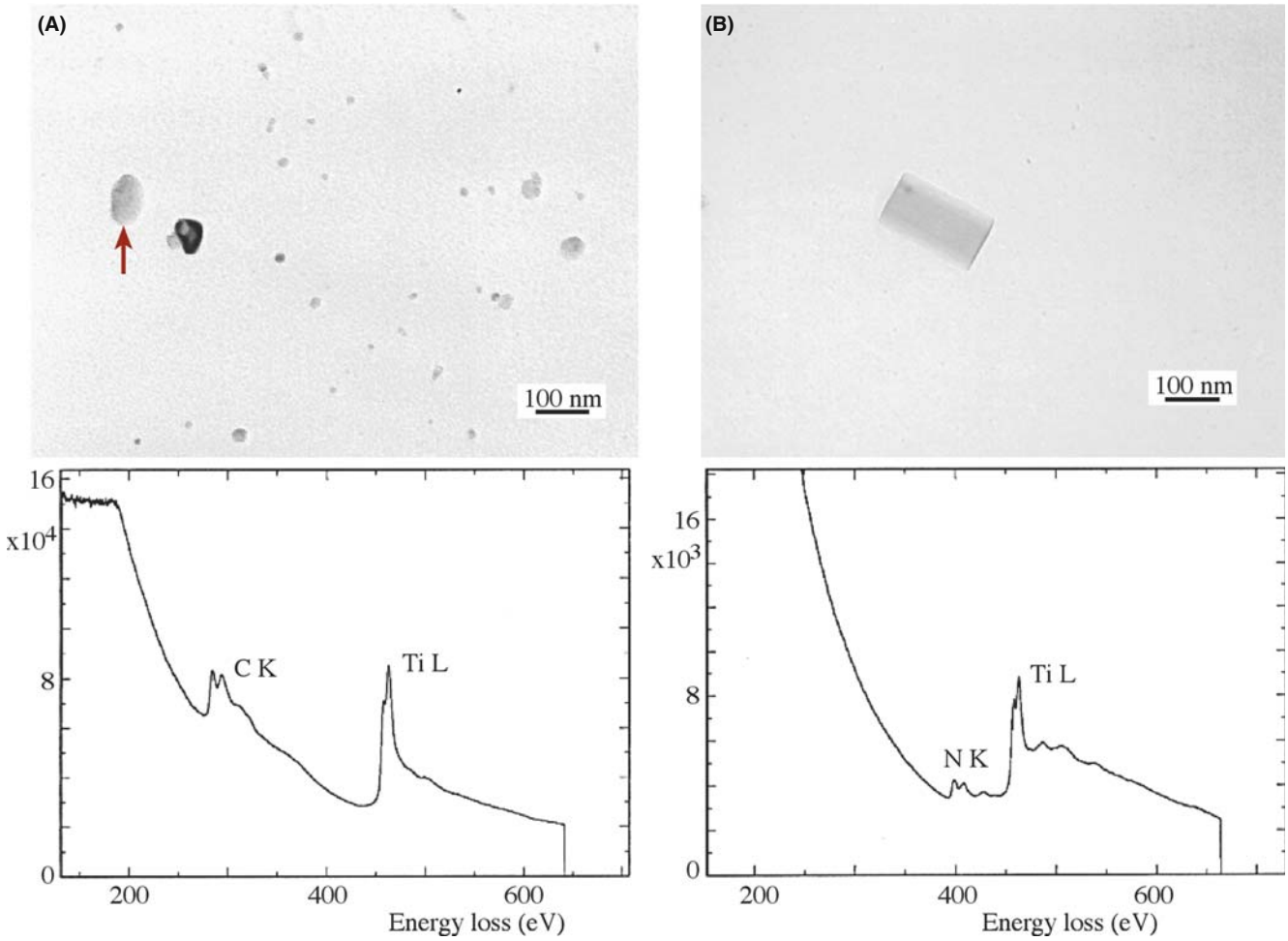

FIGURE 39.8. Images of small precipitates on an extraction replica from a stainless steel specimen, and the corresponding ionization edges showing qualitatively the presence of Ti, C, and N. Thus the precipitates can be identified as (A) TiC and (B) TiN, respectively.

you'll see how an ionization edge is built up from several contributions. The process of quantification in essence involves stripping away (or ignoring) the various contributions until you're left with Figure 39.2A, which contains the single-scattering or hydrogenic-edge intensity.

39.4.A Derivation of the Equations for Quantification

The equations we use for quantitative analysis and imaging have been derived, refined, and applied by Egerton and co-workers. The following derivation is a summary of the full treatment by Egerton given in his textbook.

We'll assume that we are quantifying a K edge, although the basic approach can be used for all edges. The K-edge intensity above background, I_K, is related to the probability of ionization, P_K, and the total transmitted intensity, I_T, by

$$I_K = P_K I_T \tag{39.1}$$

This equation assumes that the intensities are measured over the complete angular range (0–4π sr), which of course, is not the case, but we'll correct this later. In a good thin specimen we can approximate I_T to the incident intensity, neglecting backscatter and absorption effects. Now, this is the *important* point: if we assume also that the electrons contributing to the edge have only undergone a single ionization event, then we can easily obtain an expression for P_k.

$$P_K = N_{\sigma K} \exp\left(-\frac{t}{\lambda_K}\right) \tag{39.2}$$

where N is the number of atoms *per unit area* of the specimen (of thickness t) that contribute to the K edge. The assumption of a single ionization (i.e., scattering) event is reasonable, given the large mean free path (λ_k) for ionization losses; and it explains why you have to make thin specimens. Assuming single scattering also means that the exponential term is very close to unity and so

$$I_K \approx N\sigma_K I_T \tag{39.3}$$

and therefore

$$N = \frac{I_K}{\sigma_K I_T} \tag{39.4}$$

Thus, we can measure the absolute number of atoms per unit area of the specimen simply by measuring the intensity above background in the K edge and dividing it by the total intensity in the spectrum multiplied by the ionization cross section. We can easily extend this expression to two edges from elements A and B, in which case the I_T drops out and we can write

$$\frac{N_A}{N_B} = \frac{I_K^A \sigma_K^B}{I_K^B \sigma_K^A} \tag{39.5}$$

Similar expressions apply to L, M edges, etc., and combinations of edges can be used. So you see that if you are quantifying more than one element, then you don't need to gather the ZLP, which saves hitting the PDA or CCD with this high-intensity signal.

In both equations 39.4 and 39.5 we assumed that we could accurately subtract the background under the edge and that we know σ. Unfortunately, as you'll see, both background subtraction and determination of σ are non-trivial. We will discuss these points later, but first we must take account of the practical realities of spectrum acquisition, and modify the equations accordingly.

- First, you can't gather the whole of the spectrum out to the beam energy, E_0, because above ~2 keV the intensity decreases to a level close to the system noise.
- Second, while ionization-loss electrons can theoretically have any energy between E_C and E_0, in practice the intensity in the edge falls to the background level within about 100 eV of the threshold, E_C.
- Third, the background-extrapolation process becomes increasingly inaccurate beyond ~100 eV.

For all these reasons, it is imperative to restrict integration of the edge intensities to some window, Δ, usually in the range 20–100 eV. So we modify equation 39.4 to give

$$I_K(\Delta) = N\sigma_K(\Delta) I_T(\Delta) \tag{39.6}$$

The term $I_T(\Delta)$ is more correctly written as $I_l(\Delta)$ where I_l is the intensity of the zero-loss (direct beam) electrons combined with the low-loss electrons over an energy-loss window Δ. Only if we have true single scattering can we use I_T and we'll discuss the conditions for this later.

As we discussed, EELS has the tremendous advantage that the energy-loss electrons are predominantly forward scattered and so you can easily gather most of the signal. So because we never manage to collect the full angular range of energy-loss electrons, we must further modify the equation by including the collection angle β and write

$$I_K(\beta\Delta) = N\sigma_K(\beta\Delta) I_l(\beta\Delta) \tag{39.7}$$

This factor $\sigma_K(\beta\Delta)$ is the partial ionization cross section.

From this equation therefore, the absolute quantification for N is given by

$$N = \frac{I_K(\beta\Delta)}{I_l(\beta\Delta)\sigma_K(\beta\Delta)} \tag{39.8}$$

For a ratio of two elements A and B, the low-loss intensity drops out again as in equation 39.5

$$\frac{N_A}{N_B} = \frac{I_K^A(\beta\Delta)\, \sigma_K^B(\beta\Delta)}{I_K B(\beta\Delta)\sigma_K^A(\beta\Delta)} \tag{39.9}$$

We can draw a direct analogy between this equation and the Cliff-Lorimer expression (equation 35.2) used in thin-film XEDS. In both cases, the composition ratio C_A/C_B or N_A/N_B is related to the intensity ratio I_A/I_B through a sensitivity factor which we call the k_{AB} factor in XEDS and which in EELS is the ratio of two partial cross sections, σ^B/σ^A.

Remember that the major assumption in this whole approach is that the electrons undergo *a single-scattering event*. In practice, it's difficult to avoid some plural scattering, although in very thin specimens the approximation remains valid, if errors of ±10–20% are acceptable. If plural scattering is significant, then it must be removed by deconvolution, which we'll discuss in Section 39.6. You should also note when using the ratio equation your analysis is a lot better if the two edges are similar in shape, i.e., both K edges, or both L edges, otherwise the approximations inherent in equation 39.9 will be less accurate.

In summary, equations 39.8 and 39.9 give us, respectively, an absolute value of the number of atoms/unit area of the specimen or a ratio of the number of atoms of the elements A and B either at a given analysis point or within a filtered image. To get this information experimentally, you have to carry out two essential steps

- Background subtraction to obtain I_K (and hence, N) for each element A, B, etc.
- Determination of the partial ionization cross section $\sigma_K(\beta\Delta)$ to get the ratio N_A/N_B.

So again, you can see why it is important to know β.

39.4.B Background Subtraction

The background is a rapidly changing continuum decreasing from a maximum intensity just after the plasmon peak at about 15–25 eV, down to a minimum at which it is indistinguishable from the system noise, typically at $\mathcal{E} > \sim 2$ keV. In addition to plural scattering, there is also the possibility of single-scattering contributions to the background from the tails of preceding ionization edges and perhaps contributions from the spectrometer itself. Because of the complexity of these contributions, it has not been possible to model the background from first principles, as is possible in XEDS using Kramers' law.

Despite the complexity of the various contributions to the background, the methods for subtraction are relatively simple. There are two ways commonly used to remove the background

- Curve fitting.
- Using difference spectra.

Curve Fitting: You select a window δ in the background before the edge onset and fit a curve to the intensity in the window. Then you extrapolate the curve over another window Δ under the edge. This process is shown schematically in Figure 39.9, and experimentally in Figure 39.10.

We assume that the energy dependence of the background has the form

$$I = A\mathcal{E}^{-r} \tag{39.10}$$

where I is the intensity in the channel of energy loss $\mathcal{E}$, and A and r are constants. The fitting parameters are only valid over a limited energy range because they depend on $\mathcal{E}$. The exponent r is typically in the range 2–5, but A can vary tremendously. We can see some trends in how r varies. The value of r decreases as

- The specimen thickness, t, increases.
- The collection angle, β, increases.
- The electron energy loss, $\mathcal{E}$, increases.

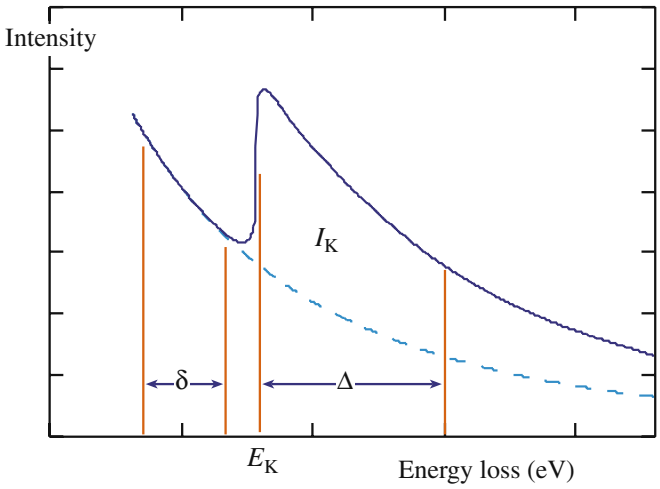

FIGURE 39.9. The parameters required for background extrapolation and subtraction under an ionization edge. The pre-edge fitting window δ is extrapolated over a post-edge window Δ then the intensity under the extrapolated line is subtracted from the total intensity in the window Δ to give the desired edge intensity I_K.

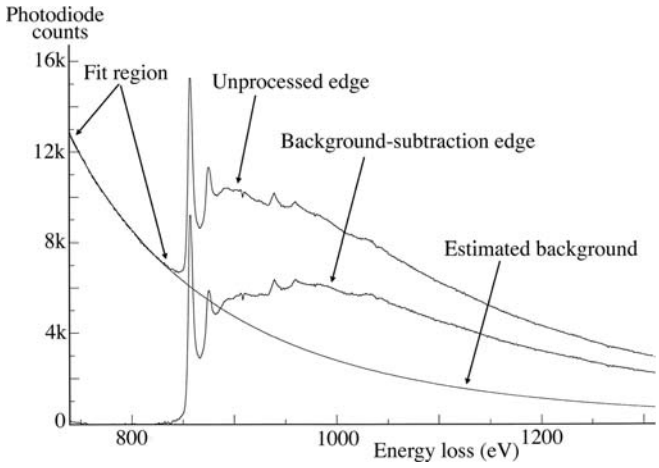

FIGURE 39.10. Comparison of an experimental Ni $L_{2,3}$ edge before and after background subtraction. The fitted region before the unprocessed edge is extrapolated to give the estimated background which is then subtracted leaving the (total) edge intensity (note: there is no edge window Δ shown here).

The fit of the curve to the tail of a preceding edge shows a similar power-law dependence to the background, and may be fitted similarly, i.e., $I = B\mathcal{E}^{-S}$. The fitting window δ should not be <10 channels and should not be >30% of E_K. In practice, however, you might not be able to fit the background over such a wide window if another edge is present within that range, which limits the goodness of fit of the curve.

You should choose the extrapolation window, Δ, such that the ratio of the finish to the start energies, $\mathcal{E}$(finish)/$\mathcal{E}$(start), is < 1.5; so Δ is smaller for lower edge energies. Using larger windows, although improving the statistics of the edge intensity, eventually reduces the accuracy of the quantification because the fitting parameters A and r are only valid over ~100 eV. If there's a lot of ELNES, either use a larger Δ to minimize its effect or avoid it in the extrapolation window unless the quantification routine can handle it.

Instead of the simple power-law fit, you can in fact use any expression, such as an exponential, polynomial, or log-polynomial, so long as it provides a good fit to the background and gives acceptable answers for known specimens. Polynomial expressions can behave erratically if you extrapolate them over a large Δ, so use them cautiously. Generally, the power law seems adequate for most purposes except close to the plasmon peaks ($\mathcal{E}$ <~100 eV). Clearly, the background channels closest

to the edge onset will influence the extrapolation most strongly, and various weighting schemes have been proposed. A noisy spectrum will be particularly susceptible to poor fitting, unless some type of weighting is used.

FITTING WINDOWS

There are two fitting windows: δ before the edge and Δ after the edge. Each has constraints for good background fitting.

We can judge the goodness of fit of a particular power-law expression qualitatively by looking at the extrapolation to ensure that it is heading toward the post-edge background and not substantially under- or over-cutting the spectrum. More quantitatively, we can assign a χ^2 value based on a linear least-squares fit to the experimental spectrum. The least squares fit can be conveniently tied in with a weighting scheme using the expression

$$\chi^2 = \sum_i \frac{(y - y_i)^2}{y^2} \qquad (39.11)$$

where y_i is the number of counts in the ith channel and $y = \ln_e I$. (Look back at Section 35.3.B.) The squared term in the denominator ensures suitable weighting of the channels close to the edge. Alternatively, the Gatan software includes 'smart' feedback which forces the background extrapolation to merge with the experimental background intensity well after the edge.

Difference Spectra: You can also remove the background using a first-difference approach (which is equivalent to differentiating the spectra). This method is particularly suited to PEELS since it simply involves taking two spectra, offset in energy by a few eV, and subtracting one from the other. As shown in Figure 39.11,

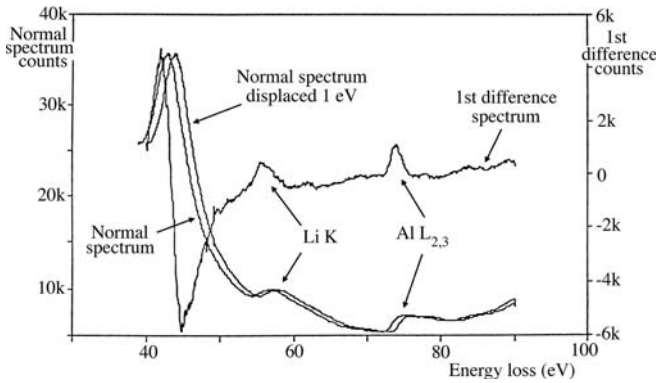

FIGURE 39.11. First-difference method of background subtraction, showing two PEELS spectra from a specimen of Al Li displaced by 1 eV and subtracted from one another to give a (first-difference) spectrum in which the background intensity falls to a straight line of close to zero counts and the small Li K and Al $L_{2,3}$ edges are clearly revealed.

the difference process results in the slowly varying background being reduced to zero and the rapidly varying ionization edge intensity showing up as classic difference peaks, similar to what you may have seen in Auger spectra. This is the *only* way to remove the background if your specimen thickness changes over the area of analysis and it also has the advantage that it suppresses spectral artifacts common to PEELS, particularly the channel-to-channel gain variation.

DIFFERENTIATE A SPECTRUM

The difference spectrum is a numerical method of differentiating the spectrum. It emphasizes changes in the spectrum.

The top-hat filter gives a second-difference spectrum. Difference and/or division are all carried out digitally.

Another kind of difference method involves convoluting the experimental spectrum with a top-hat or similar filter function, as we described in Section 35.3 for XEDS (Michel and Bonnet). Top-hat filtering effectively gives a second-difference spectrum which also removes the background but exacerbates some artifacts.

Background subtraction for energy-filtered imaging can be achieved in several ways.

The first and most usual method of background subtraction while filtering, is called the three-window method (Jeanguillaume et al. 1978). Two pre-edge windows are used to calculate the background fit and one post-edge window in which the extrapolated background is subtracted from the total intensity to leave the edge intensity (equivalent to adding another pre-edge window in Figure 39.9). Egerton has shown that the intensity in the background window under the edge (I_b) is related to the intensity in the two pre-edge windows (I_1 and I_2) by

$$I_b = [A/(1-r)][E_h^{1-r} - E_l^{1-r}] \qquad (39.12)$$

where A and r are the usual factors in the background-fitting equation (39.10) determined from I_1 and I_2 and E_h and E_l are the high- and low-energy values defining the extrapolation window under the edge. To factor out the thickness effects, a low-loss image has to be acquired and divided into the K edge image, as in equation 39.8. Alternatively, two edges can be quantified and divided to give relative quantitative images, as in the quantification equation 39.9. Selection of the energy windows and choice of their width are subject to all the limitations we discussed for background subtraction and peak integration in that same section. Because the specimen thickness will often vary over the area being imaged, this method must be applied at every pixel in the image.

METHODS FOR BACKGROUND SUBTRACTION
The three-window method: use two pre-edge windows to calculate a background.
The jump ratio: calculate by dividing two signals.
Maximum-likelihood: when you only have a few channels to use for the subtraction.

The second method that is the commonly used method is to simply divide the signal in the edge by the signal in a background window just preceding the edge. These so-called jump-ratio images are only qualitative but give useful information, as we'll see in Section 39.9.

The third background-subtraction approach often used in ETEM imaging is the maximum-likelihood method (Unser et al.), which is useful when only a few channels are available for estimating the background and the peak intensity.

Kothleiner and Hofer describe the various parameters that control your choice of the best three windows. In general, many of the considerations for the selection of δ and Δ for spectral acquisition also apply during imaging.

39.4.C Edge Integration

The edge integration procedure you use depends on how you removed the background. If you used a power-law approach, then remember that there is a limit over which the edge integration window Δ is valid. The value of Δ should be large enough to maximize the integrated intensity, but not so large that the errors in your background extrapolation dominate. Often the presence of another edge limits the upper end of the integration window. The lower end is usually defined from the edge onset, E_K, but if there is strong (well defined) near-edge structure, such as in the B K edge or the Ca L_{23} edge, then your integration window should start at an energy above these, unless the quantification schemes can handle ELNES (see below). If you subtracted the background using a first-difference approach, then you determine the peak intensity by fitting the experimental spectrum to a reference spectrum from a known standard using multiple least-squares fitting. We'll talk more about this when we discuss deconvolution of spectra.

39.4.D The Partial Ionization Cross Section

There are several ways we can determine the partial ionization cross section, $\sigma(\beta\Delta)$. We either use a theoretical approach or compare the experimental spectra with known standard spectra.

Theoretical calculation: The most common approach is that due to Egerton (the 1979 and 1981 papers) who produced two short computer programs to model the K and L shell partial cross sections. The programs are called SIGMAK and SIGMAL, respectively. They are public-domain software, have been updated regularly, and are stored in your EELS computer system. They are standard parts of the Gatan software. The codes are given in the appendices of Egerton's book. The cross sections are modeled by approximating the atom in question to an isolated hydrogen atom with a charge on the nucleus equal to the atomic number Z of the atom, but with no outer-shell electrons.

At first sight, this so-called hydrogenic cross section is an absurd approximation! The approach is actually tractable because the hydrogen-atom wave function can be expressed analytically by Schrödinger's wave equation, which can be modified to account for the increased charge on atoms above hydrogen. Because this treatment neglects the outer-shell electrons, it is best suited to K shell electrons. Figure 39.12 shows comparison between the measured nitrogen-K intensity and that computed using SIGMAK. As you can see, the SIGMAK hydrogenic model essentially ignores the near-edge and post-edge fine structure (which would be absent in the spectrum from a hydrogen atom), but still gives a reasonably good fit to the experimental edge. Figure 39.13 compares the Cr L edge with the SIGMAK model. The L shell fit is almost as good as the K fit, although the white lines are imperfectly modeled. These programs are very widely used since they are simple to understand and easy and quick to apply. An alternative approach uses empirical parameterized equations to modify σ for the effects of β and Δ; Egerton gives the appropriate codes which you can also download from URL #2.

There are more complex methods which calculate the cross section in a more realistic way than the

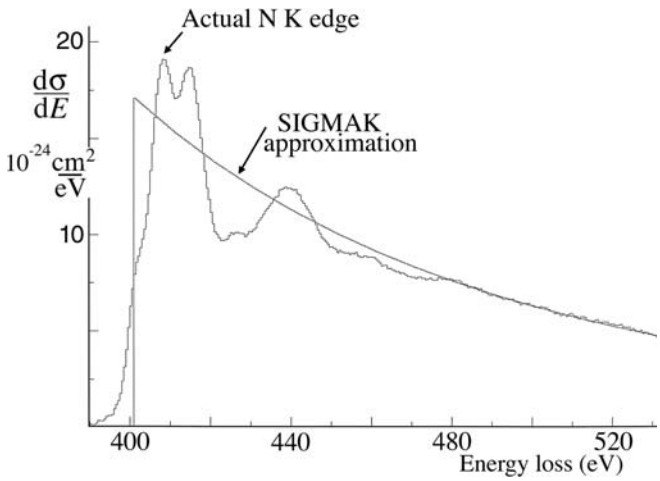

FIGURE 39.12. Comparison between an experimental N-K edge and a hydrogenic fit to the edge obtained using the SIGMAK program. The fit makes no attempt to model the near-edge fine structure but the total area under the fit is still a close approximation to the area under the experimental edge.

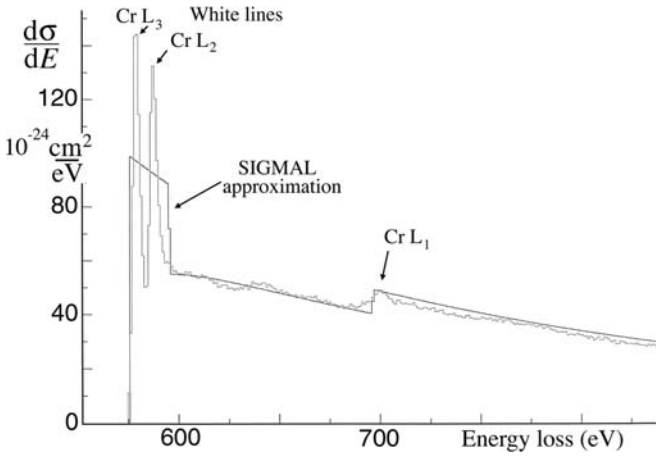

FIGURE 39.13. Comparison between an experimental Cr $L_{2,3}$ edge and a hydrogenic fit obtained using the SIGMAL program. The fit makes no attempt to model the intense white lines, but only makes a rough estimate of their average intensity.

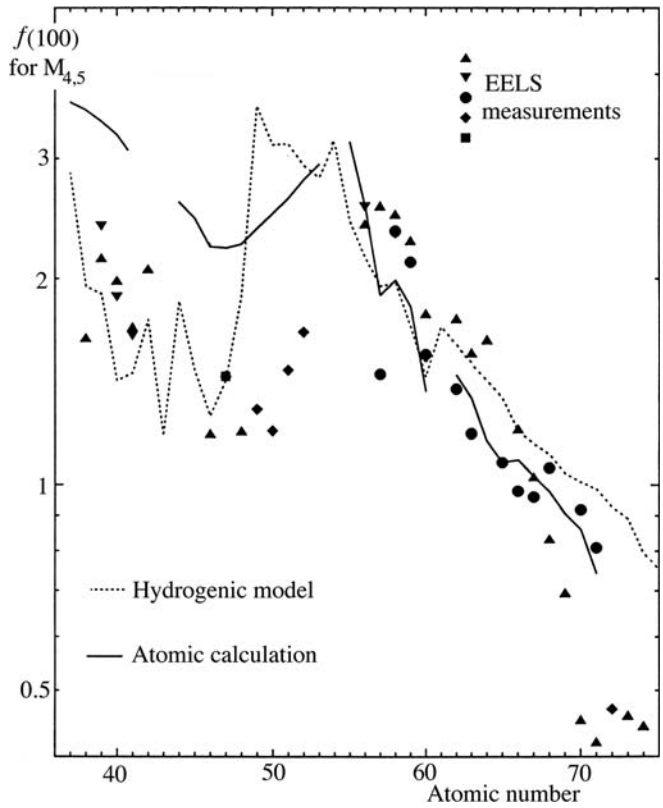

FIGURE 39.14. Comparison of the experimental and theoretical approaches to determination of the $M_{4,5}$ ionization cross section shown in terms of the variation in the dipole oscillator strength (*f*) as a function of atomic number.

SIGMAK/L hydrogenic models, e.g., using the Hartree-Slater model which is available in the Gatan software or atomic-physics approaches which are better for the more complex L and M (and even N) edges (see papers by Rez and Hofer et al.). Egerton has compared experimental and theoretical cross sections; the M shell data (which are the worst case) are shown in Figure 39.14. The data are actually plotted in terms of the oscillator strength γ (which is a measure of the response of the atom to the incident electron). This term is the integral of the generalized oscillator strength (GOS), which is proportional to the differential cross section, so just think of γ as being proportional to σ. There is still relatively poor agreement between experiment and theory for the M shell. Note that the models in Figure 39.14 are all atomic rather than hydrogenic. Similar data in Egerton's paper show better agreement for K and L shells. These models, while more precise, require substantially longer computing time but this is fast becoming less of a problem. Given the other sources of error in EELS analysis, you rarely need to go to such lengths to obtain a better value of $\sigma(\beta\Delta)$ and, unless you are well versed in the physics of ionization cross sections, you should probably stick with the SIGMAK/L methods, particularly for routine quantification.

Experimental Determination: Rather than calculating σ theoretically, you can generate a value experimentally using known standards. This approach is of course exactly analogous to the experimental *k*-factor approach for XEDS quantification in which the cross section is automatically included (along with the fluorescence yield and other factors). It is surprising at first sight that the classic XEDS approach of using standards has not been widely used in EELS, but the reason is obvious when you remember the large number of variables that affect the EELS data. The standard and unknown must have the same thickness, the same bonding characteristic, and the spectra must be gathered under identical conditions; in particular β, Δ, E_0, and t must be the same. So your standard would basically be your unknown!

Again, it is the problem of thickness measurement that appears to be the main limitation to improving the accuracy of analysis.

In summary, there are two approaches to the determination of $\sigma(\beta\Delta)$: theoretical calculation and experimental measurement. In contrast to XEDS, the theoretical approaches dominate. There is good evidence that, particularly for the lighter elements, for which EELS is best suited, the simple and quick hydrogenic model is usually adequate. However, for the heavier elements, where the M shell is used for analysis, the calculations are getting better although for such elements, it's still probably better to revert to X-ray analysis. Leapman has given a lucid and much more detailed description of the various methods of background subtraction and peak integration necessary for quantification.

One last point worth noting is that, before carrying out an experiment or gathering a long spectrum image for quantification, it is worth simulating the spectra to see if the experiment will produce useful data. We

described the advantages of DTSA for similar aspects of XEDS data in Chapter 33 and the companion text chapter. Gatan offers the EELS Advisor software (URL #3) to help take the uncertainty out of your planned experiment. Like DTSA, the EELS advisor allows you to simulate both spectra and images and will let you know if the element you seek will be detectable under your planned experimental conditions. It may tell you that the specimen is too thick or the amount of the element is below the detection or spatial resolution limits and that you need to change one or more of the many experimental variables that you have at your disposal.

39.5 MEASURING THICKNESS FROM THE CORE-LOSS SPECTRUM

While you may think we're now in a position where we have all the data needed to solve the quantification equations 39.8 and 39.9, our assumption all along has been that the spectra were the result of single scattering and we neglected plural scattering. In practice, there will *always* be some plural-scattering contribution to the ionization edges.

COMBINATION

The combination of a plasmon interaction and an ionization will show up as a bump about 15–25 eV past the onset of the edge.

This effect is shown schematically back in Figure 39.2E. So how do we go about correcting this? We can either make our specimens so thin that plural scattering is negligible or we can deconvolute the spectra. The former approach is better but sometimes unrealistic. The latter approach is mathematically simple but, as we've taken pains to point out on several occasions, deconvolution can be misleading and create spectral artifacts if not done properly; so we need to examine deconvolution in more detail. First, let's look at how we determine t because EELS offers us a simple method for this.

We saw back in Section 38.3.C that the plasmon-peak intensity is a measure of the specimen thickness but there is also thickness information in any energy-loss spectrum since the *total* amount of inelastic scatter increases with specimen thickness. So we can write a parallel expression to equation 38.7

$$t = \lambda \ln \frac{I_t}{I_0} \qquad (39.13)$$

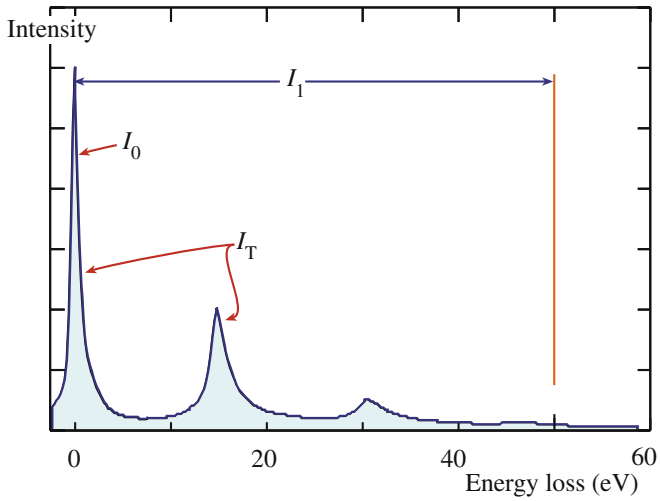

FIGURE 39.15. Definition of the zero-loss counts (I_0) and the total counts (I_T) required for thickness determination. I_T is effectively equivalent to the low-loss counts (I_l) out to ~50 eV, including I_0.

where I_0 is the ZLP intensity, I_t is the total intensity in the low-loss spectrum out to 50 eV, including I_0 (as shown in Figure 39.15) and λ is the average mean free path for these low-energy losses. We ignore any intensity above ~50 eV because, even though that's where all the interesting ionization edges are, it is a negligible fraction of I_t (as is apparent if you go back and look at Figure 37.1). To determine λ in equation 39.13, we use a parameterization based on many experimental measurements (Malis et al.)

$$\lambda = \frac{106F(E_0/E_m)}{\ln(2\beta E_0/E_m)} \qquad (39.14)$$

where λ is in nm, E_0 in keV, β in mrad, F is a relativistic correction factor, and $\mathcal{E}_m$ is the average energy loss in eV which, for a material of average atomic number Z, is given by

$$\mathcal{E}_m = 7.6\, Z^{0.36} \qquad (39.15)$$

The relativistic factor (F) is given by

$$F = \frac{1 + E_0/1022}{(1 + E_0/511)^2} \qquad (3.16)$$

You can easily store these equations in the TEM computer or in your calculator and they give t with an accuracy of ~±20 % so long as the β is < ~15 mrads at 100 keV. In addition to this and the plasmon-peak-intensity approach, there are other methods (in Egerton's book) for determining thickness from various aspects of the EEL spectrum, but Malis' parameterization method is by far the most widely used. From what you've learned so far it should be obvious that if you can determine a thickness by comparing the intensity in two

regions of the spectrum, we can just as easily form an image from each of the two intensities in equation 39.13, and thus extract a thickness image as we did for XEDS in Figure 36.13C.

You may find that, when you measure t, Murphy's law is operating and the area you're interested in is too thick for quantitative core-loss analysis. Then you'll have to deconvolute the spectra to make the single-scattering assumption valid.

39.6 DECONVOLUTION

We saw back in Figure 39.2 that the plural scattering adds intensity to the ionization edge, mainly as a result of combined inner (ionization) and outer-shell (plasmon) losses.

We can approximate the experimental ionization edge as a true single-scattering (hydrogenic) edge convoluted with the plasmon, or low-loss, spectrum.

The aim of deconvolution therefore, as shown schematically in Figure 39.16, is to extract the single-scattering contribution from the plural-scattering intensity in the spectrum. We'll describe two methods, the Fourier-Log and the Fourier-Ratio, both developed in Egerton's book and available for download at URL #1. Both methods are also incorporated in the Gatan software. Using a small β increases the deconvolution error since the plural-scattered electrons have a wide angular distribution and so more of them are excluded as β decreases.

The Fourier-Log method removes the effects of plural scattering from the whole spectrum. The technique describes the spectrum in terms of the sum of individual scattering components, i.e., the zero loss (elastic contribution) plus the single-scattering spectrum plus the double-scattering spectrum, etc. Each term is convoluted with the instrument response function, which is a measure of how much the spectrometer degrades the generated spectrum; in the case of a PEELS, this is the point-spread function we described in Section 37.5. The Fourier transform of the whole spectrum (F) is then given by

$$F = F(0)\exp\left(\frac{F(\mathcal{E})}{I_0}\right) \qquad (39.17)$$

where $F(0)$ is the transform of the elastic contribution, $F(\mathcal{E})$ is the single-scattering transform and I_0 is the zero-loss intensity. So to get the single-scattering transform you take logarithms of both sides, hence, the name of the technique.

Extracting the single-scattering spectrum would ideally involve an inverse transformation of $F(\mathcal{E})$, but this results in too much noise in the spectrum. There are various ways around this problem, the simplest of which is to approximate the zero-loss peak to a delta function. After deconvolution, you can subtract the background in the usual way, prior to quantification.

DECONVOLUTION METHODS

The Fourier-Log method: deconvolute then subtract background.
The Fourier-Ratio technique: subtract background then deconvolute.
Multiple least-squares fitting: when the specimen is not uniformly thin.
All three methods are approximations.

The danger of any deconvolution is that you may introduce artifacts into the single-scattering spectrum, e.g., from artifacts in the original spectrum. Despite the

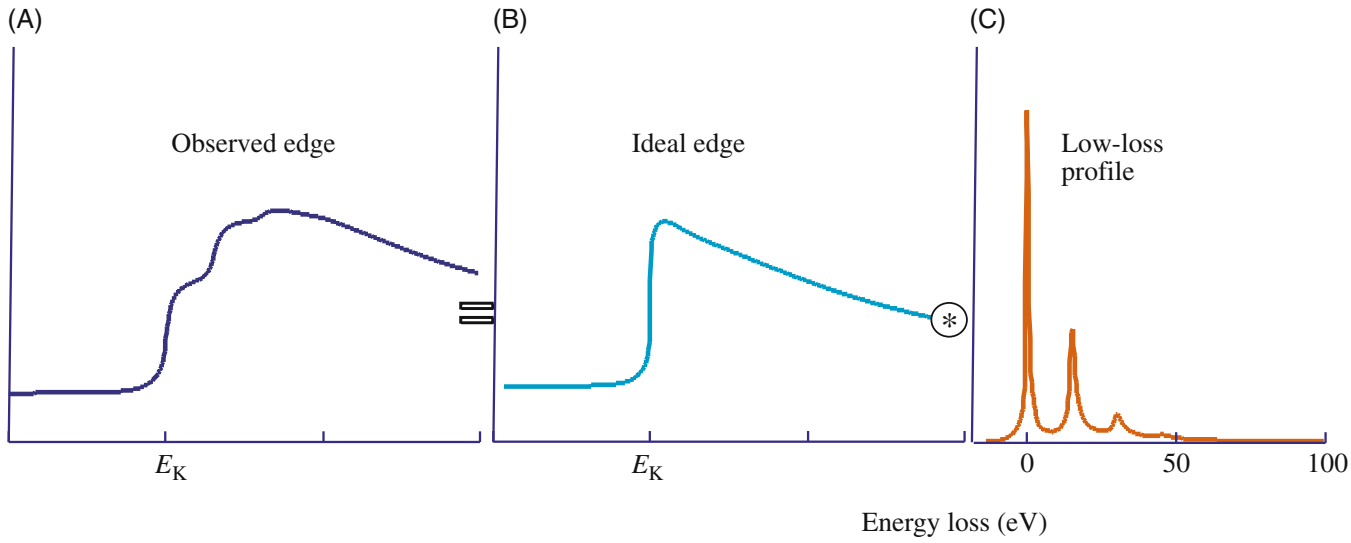

FIGURE 39.16. The experimentally observed ionization-edge intensity (A) consists of the convolution of the hydrogenic single-scattering ionization edge intensity (B) with the low-loss plasmon intensity profile (C).

assumptions and approximations, the net result of deconvolution is often an increase in the ionization-edge jump ratio. This improvement is important when you are attempting to detect small ionization edges from trace elements, or the presence of edges in spectra from thick specimens. An example of Fourier-Log deconvolution is shown in Figure 39.17.

The Fourier-Ratio technique: This approach approximates the experimental spectrum to the ideal single-scattering spectrum $F(\mathcal{E})$, convoluted with the low-loss spectrum. We define the low-loss portion of the spectrum as the region up to ~50 eV, including the ZLP, but before the appearance of any ionization edges. So we can now write

$$F' = F(\mathcal{E}) \cdot F(P) \qquad (39.18)$$

where F' is the Fourier transform of the experimental intensity distribution around the ionization edge and $F(P)$ is the Fourier transform of the low-loss (mainly plasmon) spectrum. In this equation, therefore, the instrument response is approximated by the low-loss spectrum rather than the ZLP. If we rearrange equation 39.18 to give a ratio (hence the name of the technique)

$$F(\mathcal{E}) = \frac{F'}{F(P)} \qquad (39.19)$$

We now obtain the single-scattering distribution by carrying out an inverse transformation. In contrast to the Fourier-Log technique, you must subtract the background intensity before deconvolution. Again, to avoid the problem of increased noise, it is necessary to multiply equation 39.19 by the transform of the ZLP.

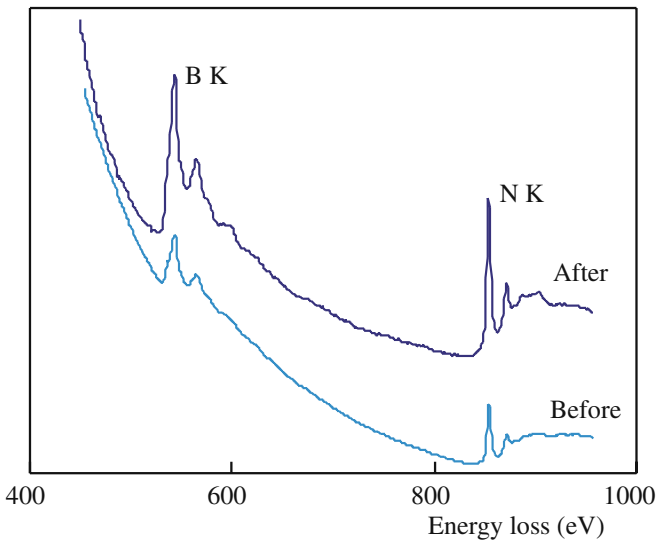

FIGURE 39.17. Spectrum from a thick crystal of BN before and after Fourier-Log deconvolution. The jump ratio in the deconvoluted spectrum (which is displaced vertically for clarity) is clearly increased by the process.

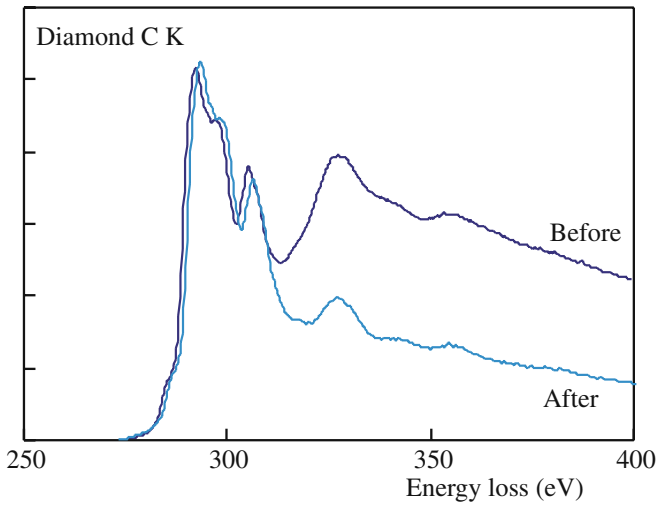

FIGURE 39.18. A carbon-K edge from a thick specimen of diamond before and after Fourier-Ratio deconvolution. You can see how the plural-scattering contribution to the post-edge structure is removed.

Figure 39.18 shows a carbon K edge after Fourier-Ratio deconvolution.

Multiple least-squares fitting: If your specimen is not uniformly thin, Fourier techniques won't work. Then you should use multiple least-squares (MLS) fitting of convoluted standard reference spectra (Leapman 2004). A single-scattering reference spectrum $R0(\mathcal{E})$ in the region of the edge to be quantified is convoluted with the first plasmon-loss portion of the unknown spectrum (P) and the resultant spectrum $R1(\mathcal{E}) = P^*R0(\mathcal{E})$ is used to generate several reference spectra ($R2(\mathcal{E}) = P^*R1(\mathcal{E})$, etc.). These reference spectra are then fitted to the experimental spectrum using MLS routines and specific fitting parameters are obtained. An experimental set of Fe, Co, and Cu reference spectra is shown in Figure 39.19A and the actual fit to part of the experimental spectrum from an intermetallic in a Cu-Be-Co alloy is shown in Figure 39.19B.

In summary, to quantify ionization-loss spectra you need a single-scattering spectrum, which can be approximated if you have very thin specimens or generated by deconvolution of your experimental spectrum. It is arguable that, given the stringency of the single approximation, it might be wise to deconvolute all core-loss spectra prior to quantification, but the uncertain effects of the possible errors introduced by deconvolution mean that you should do this cautiously. Often you'll find it useful to deconvolute the point-spread junction from all PEELS spectra, since this sharpens the edge onset and any ELNES intensity variations.

DECONVOLUTION CAUTION

Always check the validity of the deconvolution routine by applying it to spectra from a known specimen obtained over a range of thickness.

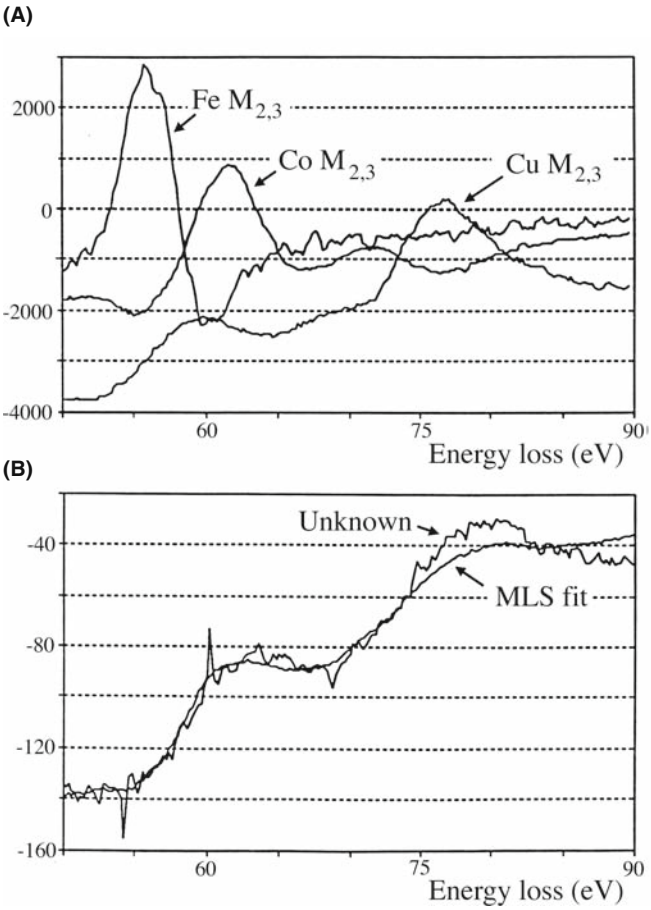

FIGURE 39.19. (A) Three first-difference low-loss, M-edge reference spectra from Fe, Co, and Cu superimposed on a low-energy portion of an experimental (first-difference) spectrum from an intermetallic particle in a Cu-Be-Co alloy. (B) MLS fit of the combined reference spectra to the experimental spectrum showing the good fit that can be obtained.

39.7 CORRECTION FOR CONVERGENCE OF THE INCIDENT BEAM

If you're working in STEM mode to get high spatial resolution, then it is possible that the beam-convergence angle α may introduce an error into your quantification. When α is equal to or greater than β, convergence effects can limit the accuracy because the experimental angular distribution of scattered electrons will be wider than expected (yet again, a good reason to know β). Therefore, you have to convolute the angular distribution of the ionization-loss electrons with the beam convergence angle. Joy (1986b) proposed handling this through a simple equation which calculates the effective reduction (R) in the partial cross section $\sigma(\beta\Delta)$ when $\alpha > \beta$.

$$R = \frac{\left[\ln\left(1 + \frac{\alpha^2}{\theta_E^2}\right)\beta^2\right]}{\left[\ln\left(1 + \frac{\beta^2}{\theta_E^2}\right)\alpha^2\right]} \qquad (39.20)$$

where θ_E is the characteristic scattering angle. A similar reduction factor is incorporated in the Gatan software quantification routines. So you can see that if α is small (particularly if it is smaller than β) then R is $<<1$ and the effect of beam convergence is negligible. Generally, with the typical range of probe-limiting apertures in a STEM, convergence angles should not be larger than 5–10 mrads so it should always be feasible to make sure that β is large enough. However, a note of caution is worthwhile because, with C_s correction, it is now possible to use much larger convergence angles to increase the probe current without degrading the probe size.

39.8 THE EFFECT OF THE SPECIMEN ORIENTATION

In crystalline specimens, diffraction may influence the intensity of the ionization edge. This effect may be particularly large if your specimen is oriented close to strong two-beam conditions and, as we saw back in Chapter 35, this can be used to good effect in ALCHEMI. Both X-ray emission and ionization-loss intensity can change because of electron channeling effects close to the Bragg condition. At the Bragg condition, the degree of beam-specimen interaction increases, compared with zone-axis illumination where no strong scatter occurs and the energy-loss processes behave similarly. This phenomenon (known as the Borrmann effect in XEDS) is not important for low-energy edges, but intensity changes of a factor of 2 have been reported for Al and Mg K edges (Taftø and Krivanek). The use of large α minimizes the problem in XEDS, but beam-convergence effects are themselves a problem in EELS as we just described. Unless you're an alchemist, the easiest way to avoid orientation effects is simply to operate under kinematical conditions and stay well away from any bend centers or bend contours, just as in XEDS.

39.9 EFTEM IMAGING WITH IONIZATION EDGES

There are countless examples of EELS analyses using ionization-loss edges in the general references that we have given at the end of this and the other EELS chapters. As we described back in Section 37.8, you have several experimental options such as point analyses, spectrum-line profiles, and various forms of energy-filtered TEM imaging. By far the most powerful method of analysis, as with XEDS, is to form EFTEM images. You can either select a given edge from which to form a single image or you can gather a spectrum image and select the specific energy later. The former method is the norm for in-column filters while the latter is more

common for post-column GIFs. We'll look at both but refer you to the 1995 text on the subject by Reimer for more theoretical and practical details and the review by Hofer and Warbichler for many illustrative examples. You can also image portions of the fine structure in the edge as we'll show in the next chapter, but here we will emphasize the power of ionization-loss analysis with reference to elemental images only. It is good to draw comparisons with what can be achieved with elemental imaging with XEDS, as we described back in Chapters 32–35.

39.9.A Qualitative Imaging

EFTEM images using the intensity in ionization edges will obviously correspond to elemental maps. The simplest way to get this information is to *subtract* a pre-edge background image from a post-edge image; this two-window subtraction method gives a passable qualitative elemental distribution. Alternatively, you can just *ratio* images of pre- and post-edge windows then what you get is called a jump-ratio image (see Figure 39.20B and C) which, again, is not quantitative and the intensity just reflects the edge to background ratio. Obviously, both of these qualitative methods will work best if (i) the jump ratio is high, (ii) the edge intensity is clearly visible above the background, and (iii) both thickness and diffraction conditions remain reasonably constant across the mapped region. Otherwise, the interpretation of any intensity changes is fraught with danger and artifacts abound. In fact, unless your specimen is very thin ($t \leq 0.1\ \lambda$) it's probably not worth bothering with this qualitative approach and you may as well spend your time forming quantitative EFTEM images.

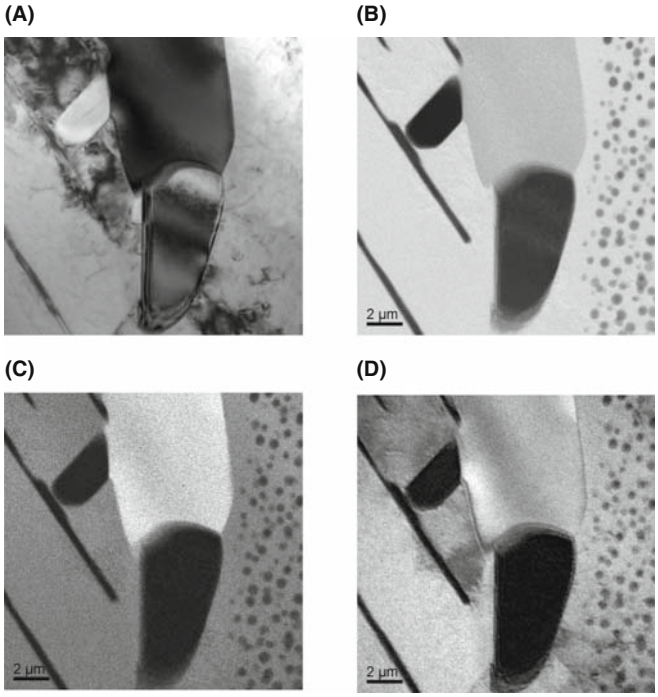

FIGURE 39.20. (A) BF image of precipitates in a stainless-steel foil. The other images were obtained from specific energy-loss electrons and illustrate both jump ratio and fully quantitative images. (B) Fe M jump ratio image; (C) Cr L jump ratio image; (D) quantitative Cr map.

39.9.B Quantitative Imaging

If, at each pixel, we carry out a background subtraction, an edge integration, and multiply the resulting intensity by the partial ionization cross section ratio, we should get quantitative images of the distribution of specific elements. There isn't too much difference, in principle, between quantifying a spectrum as we've just described in equations 39.8 and 39.9 and forming an image. The main difference is in fact in the method of background subtraction, which we've also described already in Section 39.4.B.

The most common method for quantitative EFTEM imaging involves acquiring three images from electrons in selected energy windows: two from the background preceding the edge and one from under the edge as we've already described. This approach works equally well for an in-column filter or for a post-column GIF; you can either operate in TEM mode and acquire three images or operate in STEM mode and choose whether you select just the three energy windows or gather a full spectrum image. The only difference is that the TEM images can be acquired in a few seconds while the STEM approach may require minutes or even hours and is probably only worth doing if you are acquiring a full spectrum image. Figure 39.20 shows ratio images and fully quantitative images pulled out of a spectrum-image data cube.

In both instruments, to form a specific filtered image, you shift the energy spectrum until the desired energy window passes through the energy-selecting slit (see the schematic diagrams in Figures 37.13 and 37.15). The energy shift is actually achieved by changing the accelerating voltage of the TEM so that electrons of different energies stay on-axis and thus in focus through the spectrometer. The quality of your images is governed by the same factors that control the spectrum: good jump ratios to get good signals, well-separated peaks to ensure good background-fitting statistics, and a good thin specimen to permit valid quantification under single-scattering conditions. Once acquired, your filtered images can be subject to advanced post-specimen processing, such as pixel-clustering methods (Cutrona et al.) or the standard methods, such as color assignments for different elements, as shown back in Figure 37.17D. If you're at all uncertain about whether the experiment will work, remember to simulate it first, using the EELS Advisor software (URL #2).

EFTEM imaging will only continue to improve as all the instrumental factors that we have already discussed become common. We will have C_s correction, monochromation, and better spectrometers with more uniform transmissivity achieved via higher-order aberration correction.

39.10 SPATIAL RESOLUTION: ATOMIC-COLUMN EELS

In contrast to the situation in XEDS, beam spreading is not a major factor in determining the source of the EELS signal and so the many factors that influence beam spreading are mainly irrelevant. The spectrometer only collects those electrons emanating from the specimen in a narrow cone, as shown in Figure 39.21 Therefore, energy-loss electrons that are elastically scattered through large angles are excluded from contributing to your spectrum. Remember that for XEDS these same high-angle electrons would still generate X-rays some distance from the incident-probe position, and these X-rays would be detected by XEDS. In the absence of a contribution from beam spreading, the spatial resolution of ionization-loss spectrometry depends on the mode of analysis

- The factor controlling the resolution in STEM mode, or in a probe-forming (diffraction) mode on a TEM, is mainly the size of the probe; because of the strong forward-scattered signal, we can easily get data with probe sizes < 0.2 nm and with aberration correction we can break the Ångstrom barrier.
- When we operate in TEM mode, the spatial resolution is a function of the selecting aperture, i.e., the spectrometer entrance aperture and its effective size at the plane of the specimen. Lens aberrations usually limit the spatial resolution, as we showed back in Section 37.4.C.

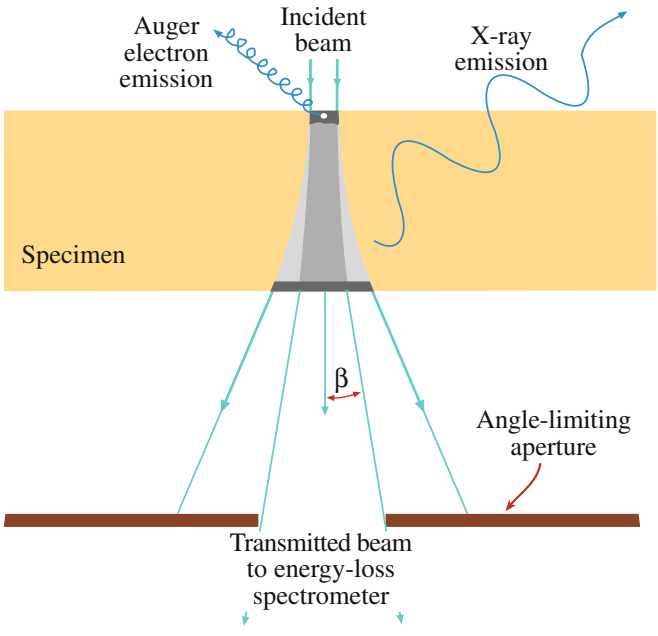

FIGURE 39.21. The effect of the spectrometer collection angle is to limit the contribution to the spectrum from high-angle scattered electrons, thus ensuring high spatial resolution. In contrast, X-rays can be detected from the whole beam-specimen interaction volume.

In addition to the usual factors affecting the probe size, such as the diffraction limit and lens aberrations (go back and read Chapter 5), another factor that we have to consider in EELS, but ignore in XEDS (although it occurs in X-ray generation also) is the phenomenon of delocalization.

DELOCALIZATION IN EELS

Delocalization is the ejection of an inner-shell electron by the passage of a high-energy electron some distance from the atom. It's as if the beam electron scares the core-shell electron sufficiently to eject it without actually laying a finger on it!

The scale of this wave-mechanical effect is inversely proportional to the energy loss over dimensions of a few nm (which, of course, is very large if you're worried about atomic-level spatial resolution). Egerton gives the following simplified expression for the diameter (d_{50}) containing 50% of the inelastic intensity

$$(d_{50})^2 = \left(\frac{0.5\lambda}{\theta_E^{3/4}}\right)^2 + \left(\frac{0.6\lambda}{\beta}\right)^2 \qquad (39.21)$$

where you should recognize all the terms and yet again appreciate the importance of knowing your collection angle. This expression gives a localization of ~1 nm for $\mathcal{E}$ = 50 eV and 0.4 nm for $\mathcal{E} \simeq 300$ V (C edge K) and might therefore appear to prevent atomic-resolution EELS. Fortunately, delocalization does not appear to be a factor in STEM images of single, isolated atoms and resolution appears to be primarily determined by the width of the probe, even for light atoms. So it appears that the usual factors, such as probe aberrations, signal to background in the EELS signal, and damage are much more important in terms of EELS spatial resolution. All the experimental evidence seems to agree with the secondary role for delocalization in that HAADF imaging of single atoms has been long established (see Section 22.4 and the companion text); atomic-level changes in chemistry were first demonstrated by ionization loss in the early 1990s (Browning et al. and Batson). The same process that confines the electron beam to channel along the atomic columns in HAADF imaging also means that the spectroscopic

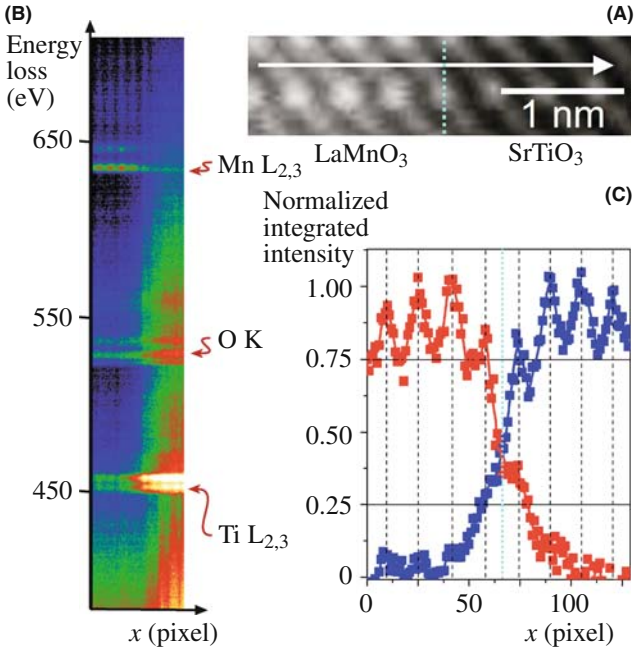

FIGURE 39.22. (A) HAADF image of a $LaMnO_3/SrTiO_3$ interface (blue dashed line). (B) EELS linescan along the arrowed direction in (A). Approximate positions of the Ti $L_{2,3}$, O K and Mn $L_{2,3}$ absorption edges are highlighted. The ripple corresponds to atomic-plane positions along the scan. (C) Normalized integrated intensities (40-eV window) under the Ti $L_{2,3}$ (blue) and the Mn $L_{2,3}$ (red) edges. Black dotted lines show the estimated positions of the respective MnO_2 and TiO_2 atomic planes.

signal is similarly localized. Because the EELS intensities are so much higher than XEDS, we are able to extract EELS spectra which contain information from a single atomic column, as shown in Figure 39.22). Both the Ti and Mn integrated signals in Figure 39.22C show an approximate decrease of 50% (or higher) within an atomic plane of the interface indicating true atomic-level resolution.

It is possible even to detect the presence of single atoms of high-Z elements on individual atomic columns of lower-Z elements (see next section) and C_s correction now makes atomic-resolution EELS almost straightforward (Varela et al.)

39.11 DETECTION LIMITS

The detection limits for ionization-loss spectrometry are governed by the same factors as we discussed for XEDS, so we have to optimize several factors

- The edge intensity.
- The signal to background ratio (jump ratio).
- The efficiency of signal detection.
- The time of analysis.

As is obvious in Figure 39.21, EELS has an inherently higher signal collection efficiency than XEDS. Conversely, as we've seen, it also has a correspondingly poorer signal to background because of the higher plural scattering. But, as for the best spatial resolution, more signal wins in the end. Leapman and Hunt argued in 1991 that, in most situations, PEELS is more sensitive to the presence of small amounts of material than XEDS. This has been borne out in experimental studies over many years and the latest improvements in FEG sources, C_s correction, and spectrometer hardware have brought us to the point where combined imaging and spectroscopic analysis (including fine structure and associated electronic effects) of single atoms is achievable. Figure 39.23 shows single-atom analytical sensitivity with atomic-level spatial resolution. So while, in principle, the inverse relationship between analytical sensitivity and spatial resolution that we described for XEDS in Figure 36.11 applies, when you're able to detect single atoms with atomic resolution you've just about reached the fundamental limit of any analytical technique.

Conclusion: analysis using ionization edges offers both atomic-resolution spatial resolution and single-atom analytical sensitivity.

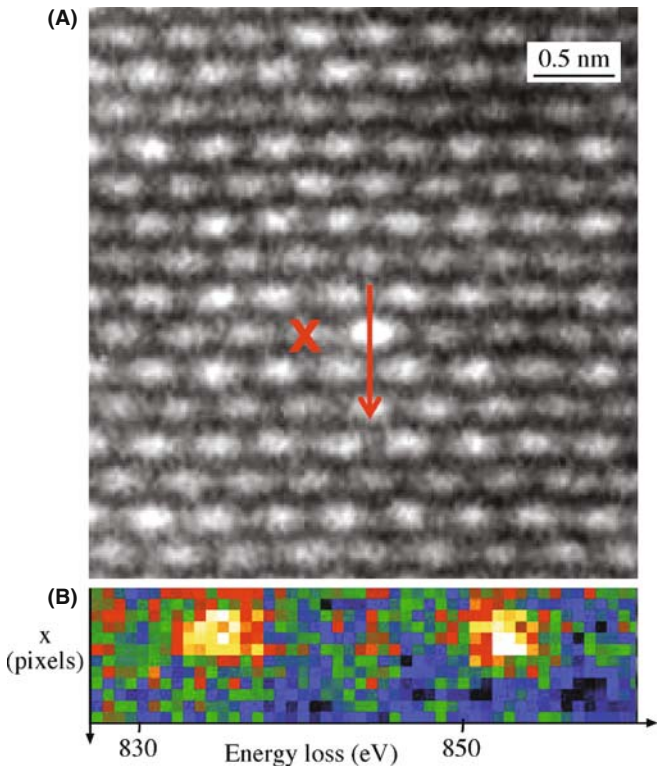

FIGURE 39.23. (A) HAADF image of a La impurity atom (X) in single atomic column in $CaTiO_3$. (B) Spectrum line-intensity profiles showing the white lines in the La $M_{4,5}$ edge as the beam scans across the La atom (along the red arrow). The white lines appear only when the La atom is scanned.

CHAPTER SUMMARY

The ionization edges can be used to give quantitative elemental analyses and quantitative images from all the elements in the periodic table, using a simple ratio equation. Beware, however, of the many experimental variables you have to define for your TEM, PEELS, energy filter, and (most importantly) your very thin specimen. Compared to XEDS there have been relatively few quantitative analyses or composition profiles measured using EELS, but quantitative imaging is becoming much more common.

To use Egerton's ratio equation you have to

- Subtract the background using a power law, or MLS approach. The former is easier. The latter is better for complex spectra.
- Integrate the edge intensity. That's usually straightforward.
- Determine the partial ionization cross section $\sigma_K(\beta\Delta)$. Calculate $\sigma_K(\beta\Delta)$ with SIGMAK and SIGMAL for most K and L edges.
- For M edges use a known standard or, better still, use XEDS.
- For the lightest elements (e.g., Li) use a known standard.

The biggest limitation to quantification is that your specimens have to be much thinner than one mean free path (typically $<<$ 50 nm) otherwise deconvolution routines are needed, which can introduce artifacts of their own.

Ionization-loss imaging is becoming widespread because of the increased availability of in-column and post-column filters and is the recommended method for quantitative analysis.

Spatial resolution and minimum detection are better than for XEDS. Combined atomic-column resolution and single-atom detection has been demonstrated.

BOOKS AND REVIEWS

Ahn, CC Ed. 2004 *Transmission Electron Energy-Loss Spectrometry in Materials Science and the EELS Atlas* 2nd Ed. Wiley-VCH Weinheim Germany. Must-read chapters on quantification and imaging.

Brydson, R 2001 *Electron Energy-Loss Spectroscopy* Bios (Royal Microsc. Soc.) Oxford UK. Great basic introduction; lots of practical tips.

Egerton, RF 1996 *Electron Energy-Loss Spectroscopy in the Electron Microscope* 2nd Ed. Plenum Press New York. Still the EELS bible. Read more here about the Bethe ridge.

Hofer, F and Warbichler, P 2004 *Elemental Mapping Using Energy-Filtered Imaging* in *Transmission Electron Energy-Loss Spectrometry in Materials Science and the EELS Atlas* 2nd Ed. **159**–233 Ed. CC Ahn Wiley-VCH Weinheim Germany. A thorough review of EFTEM/ESI, full of outstanding examples.

Joy, DC 1986a *The Basic Principles of EELS,* 1986b *Quantitative Microanalysis using EELS* in *Principles of Analytical Electron Microscopy* 249–276 and 277–299 Eds. DC Joy, A. Romig Jr. and JI Goldstein Plenum Press New York. Introduction to the principles and in-depth discussion of the experimental details necessary for quantification

Kohler-Redlich, P and Mayer, J 2003 *Quantitative Analytical Transmission Electron Microscopy* in *High-Resolution Imaging and Spectrometry of Materials* 119–187 Eds. F Ernst and M Rühle Springer New York. Integrated review of quantitative EELS and other TEM techniques with an emphasis on interfacial studies.

Reimer, L Ed. 1995 *Energy-Filtering Transmission Electron Microscopy* Springer New York. The first book on EFTEM/ESI with all you need to know about the theory and practice, but very few applications.

APPLICATIONS

Batson, PE 1993 *Simultaneous STEM Imaging and Electron Energy-Loss Spectroscopy with Atomic-Column Sensitivity* Nature **366** 727–728.

Browning, ND Chisholm, MF and Pennycook, SJ 1993 *Atomic-Resolution Chemical Analysis Using a Scanning Transmission Electron Microscope* Nature **366** 143–146.

Cutrona, J, Bonnet, N, Herbin, M and Hofer, F 2005 *Advances in the Segmentation of Multi-Component Microanalytical Images* Ultramicrosc. **103** 141–152.

Egerton, RF 1979 *K-Shell Ionization Cross-Sections For Use in Microanalysis* Ultramicrosc. **4** 169–179.

Egerton, RF 1981 *SIGMAL; A Program For Calculating L-shell Ionization Cross-Sections* in *Proc. 39th EMSA Meeting*198–199 Ed. G.W. Bailey Claitors Baton Rouge LA.
Egerton, RF 1993 *Oscillator-Strength Parameterization of Inner-Shell Cross Sections* Ultramicrosc. **50** 13–28.
Hofer, F, Golob, P and Brunegger, A 1988 *EELS Quantification of the Elements Sr to W by Means of M_{45} Edges* Ultramicrosc. **25** 81–84.
Jeanguillaume, C, Trebbia, P and Colliex, C 1978 *About the Use of Electron Energy-Loss Spectroscopy for Chemical Mapping of Thin Foils with High Spatial Resolution* Ultramicrosc. **3** 237–249.
Leapman, RD and Hunt, JA 1991 *Comparison of Detection Limits for EELS and EDXS* Microsc. Microanal. Microstruct. **2** 231–244.
Leapman RD (2004) *EELS Quantitative Analysis* in *Transmission Electron Energy Loss Spectrometry in Materials Science and the EELS Atlas* 2nd Ed. 49–96 Ed CC Ahn Wiley-VCH Weinheim Germany. A great reference source.
Malis, T, Cheng, S and Egerton, RF 1988 *EELS Log-Ratio Technique for Specimen-Thickness Measurement in the TEM* J. Electron Microsc. Tech. **8** 193–200.
Michel, J. and Bonnet, N 2001 *Optimization of Digital Filters for the Detection of Trace Elements in EELS. III – Gaussian, Homomorphic and Adaptive Filters* Ultramicrosc. **88** 231–242.
Muller, DA and Silcox, J 1995 *Delocalization in Inelastic Scattering* Ultramicrosc. **59** 195–213. If you're physics-oriented and want to read more about delocalization in EELS.
Rez, P 2003 *Electron Ionization Cross Sections for Atomic Subshells* Microscopy and Microanalysis **9** 42–53.
Taftø, J and Krivanek, OL 1982 *Site-Specific Valence Determination by Electron Energy-Loss Spectroscopy* Phys. Rev. Lett. **48** 560–563.
Unser, M, Ellis, JR, Pun, T and Eden, M 1986 *Optimal Background Estimation in EELS* J. Microsc. 145 245–256.
Varela, M, Lupini, AR, van Bentham, K, Borisevich, AY, Chisholm, MF, Shibata, N, Abe, E and Pennycook, SJ 2005 *Materials Characterization in the Aberration–Corrected Scanning Transmission Electron Microscope* Annu. Rev. Mater. Res. **35** 539–569.

URLs

1) http://www.cemes.fr/&7Eeelsdb/
2) http://laser.phys.ualberta.ca/∼egerton/programs/programs.htm3.
3) http://www.gatan.com/software/eels_advisor.php

SELF-ASSESSMENT QUESTIONS

Q39.1 Is it better to do ionization–loss analysis at 100 keV or 200 keV? Justify your answer.
Q39.2 Why should you not operate with too small a collection angle if attempting to do quantitative analysis?
Q39.3 Why should you not operate with too large a collection angle if attempting to do quantitative analysis?
Q39.4 What is the compromise you make when choosing a large or small collection angle?
Q39.5 What kind of energy resolution do you need for quantitative analysis. Does this resolution requirement permit you to improve other aspects of the spectral acquisition?
Q39.6 Define the jump ratio. How can you increase this ratio for a given ionization edge?
Q39.7 Why do we not define the ionization edge energy as the peak-intensity channel of the edge?
Q39.8 What are white lines and why are they called this?
Q39.9 Define N, I, σ, and δ, including the appropriate units.
Q39.10 What relationship exists (if any) between the background-fitting window and the background-extrapolation window?
Q39.11 Under what circumstances might you use a 'goodness of fit' criterion for the background-extrapolation procedure?
Q39.12 Why do we use the term 'partial ' to describe the ionization cross section (σ) used in the Egerton equation?
Q39.13 Why do the simplistic SIGMAK and SIGMAL models still give a reasonable approximation to fitting the edge intensity?
Q39.14 Why isn't there a SIGMAM model and in its absence, how do you quantify M edges?
Q39.15 Why would you deconvolute your spectrum before attempting to quantify it?
Q39.16 Why is the background subtraction procedure in EELS far more important and difficult than in XEDS?
Q39.17 What are the units of quantification of the specimen composition obtained via the ratio method?
Q39.18 What is the greatest uncertainty in the quantification procedure?
Q39.19 Why might you need to correct the partial ionization cross section for too large a convergence angle instead of simply decreasing the C2 aperture?
Q39.20 Why is the spatial resolution of EELS fundamentally better than that of XEDS?

Q39.21 What is delocalization and how might it affect your EELS analysis?
Q39.22 Why do we call an ideal edge 'hydrogenic'?
Q39.23 Why does a hydrogenic ionization edge look like a triangle?
Q39.24 Why don't we see ionization edges from core levels much deeper than about 2 keV?

TEXT-SPECIFIC QUESTIONS

T39.1 Explain the nomenclature in Figure 39.1.
T39.2 Examine Figure 38.1 and compare with Figure 39.3. Why are both the zero loss and plasmon loss peaks effectively Gaussian in shape when all the ionization edges have a much broader intensity distribution extending asymmetrically over several tens of eV?
T39.3 Is the background intensity as drawn in Figure 39.2 realistic and if not, why not?
T39.4 If the energy resolution of the EELS spectrometer is on the order of a few eV at worst, why is it not possible to discriminate ionization edges that are several tens of eV apart without resorting to deconvolution?
T39.5 Given that TiN and TiC have equal numbers of atoms of each elemental constituent, why are the intensities so very different in the EELS spectra in Figure 39.8? What other spectroscopic method might you use to distinguish TiC and TiN, and why can't this method be used in an AEM?
T39.6 Does the first difference approach (Figures 39.10 and 39.19) actually remove the background intensity? If not, why not? How does this method compare with the top-hat filter approach used in XEDS?
T39.7 Why do we recommend using experimental standards for the best *k*-factor determination in XEDS but generally prefer calculation of partial ionization cross section values for EELS quantification?
T39.8 Calculate the thickness of an Fe specimen for which the low-loss intensity is 10% of the zero-loss intensity in a spectrum gathered with a collection angle of 100 mrads at 100 keV.
T39.9 Compare and contrast the two principal methods of deconvolution in Figures 39.17 and 39.18.
T39.10 Why can't we simply expand the integration windows δ and Δ in Figure 39.9 in order to increase the goodness of fit of the background subtraction and increase the total number of counts in the edge, respectively?
T39.11 Compare and contrast the expression for quantification of an ionization-loss spectrum (equation 39.5) with the Cliff-Lorimer expression for quantification of a characteristic X-ray spectrum (equation 35.2).
T39.12 Justify using the gross simplifications of the hydrogenic approach to model ionization edges shown in Figures 39.12 and 39.13.
T39.13 Look at Figure 39.6 and explain the relationship between the penetration of the electron into the potential well and the value of the energy loss.
T39.14 List the pros and cons of deconvoluting out the plural-scattering contributions and the point-spread function from a spectrum.
T39.15 Calculate the maximum convergence angle (α) you should use, such that the cross section for carbon K shell ionization (100 kV, $\beta = 20$ mrad) needs no correction. State any assumptions.
T39.16 Why has the spatial resolution of EELS analysis received so little study compared to that of X-ray analysis?
T39.17 Compare and contrast two different background-subtraction methods used for EFTEM with two different methods used for spectroscopy.
T39.18 Compare and contrast the experimental factors that limit spatial resolution in XEDS and EELS.
T39.19 Compare and contrast the experimental factors that limit analytical detection limits in XEDS and EELS.
T39.20 How do you know if your specimen is too thick for EELS analysis and how do you minimize the problem (apart from making a thinner specimen)?
T39.21 Why is EELS so much more efficient at collecting electrons compared to XEDS collecting X-rays, as summarized in Figures 39.4 and 39.5, given that the actual collection angles are about the same?
T39.22 Why is the B K edge so much more intense than the N K edge in Figure 39.3 when the atomic ratio of B:N in boring nitride is 1:1?
T39.23 What is a typical collection angle for X-rays in an XEDS spectrometer and how does it compare with the collection angle for electrons in an EELS?